Journal of Materials Chemistry B

ROYAL SOCIETY OF CHEMISTRY

PAPER

View Article Online
View Journal | View Issue

Cite this: J. Mater. Chem. B, 2024, 12, 6351

Dry and wet wrinkling of a silk fibroin biopolymer by a shape-memory material with insight into mechanical effects on secondary structures in the silk network†

Elizabeth Oguntade,[ab] Caleb Wigham,[cd] Luiza Owuor,[ab] Ujjwal Aryal,[ab] Kerrin O'Grady,[ab] Anthony Acierto,[ab] R. Helen Zha[cd] and James H. Henderson *[ab]

Surface wrinkling provides an approach to modify the surfaces of biomedical devices to better mimic features of the extracellular matrix and guide cell attachment, proliferation, and differentiation. Biopolymer wrinkling on active materials holds promise but is poorly explored. Here we report a mechanically actuated assembly process to generate uniaxial micro-and nanosized silk fibroin (SF) wrinkles on a thermo-responsive shape-memory polymer (SMP) substrate, with wrinkling demonstrated under both dry and hydrated (cell compatible) conditions. By systematically investigating the influence of SMP programmed strain magnitude, film thickness, and aqueous media on wrinkle stability and morphology, we reveal how to control the wrinkle sizes on the micron and sub-micron length scale. Furthermore, as a parameter fundamental to SMPs, we demonstrate that the temperature during the recovery process can also affect the wrinkle characteristics and the secondary structures in the silk network. We find that with increasing SMP programmed strain magnitude, silk wrinkled topographies with increasing wavelengths and amplitudes are achieved. Furthermore, silk wrinkling is found to increase β-sheet content, with spectroscopic analysis suggesting that the effect may be due primarily to tensile (*e.g.*, Poisson effect and high-curvature wrinkle) loading modes in the SF, despite the compressive bulk deformation (uniaxial contraction) used to produce wrinkles. Silk wrinkles fabricated from sufficiently thick films (roughly 250 nm) persist after 24 h in cell culture medium. Using a fibroblast cell line, analysis of cellular response to the wrinkled topographies reveals high viability and attachment. These findings demonstrate use of wrinkled SF films under physiologically relevant conditions and suggest the potential for biopolymer wrinkles on biomaterials surfaces to find application in cell mechanobiology, wound healing, and tissue engineering.

Received 16th January 2024,
Accepted 6th June 2024

DOI: 10.1039/d4tb00112e

rsc.li/materials-b

1. Introduction

Surface wrinkling, a phenomenon frequently observed in natural systems,[1–3] has in recent years been studied as a means of producing topographies that may mimic features of the extracellular matrix (ECM) and can direct cell behaviors. Wrinkles have been shown to affect cellular morphology,[4] alignment,[4] and phenotypic expression of cells.[5] More broadly, and depending on the environment in which they are being applied, wrinkles can control adhesion and wetting, act as flow channels, or contribute to stretching or mechanical integrity of materials,[6] making them broadly useful for application in microfluidic devices,[7] stretchable electronics,[8] precision metrology,[8] and smart adhesion.[9]

A common approach for bottom-up fabrication of surface wrinkles is buckling of a thin film.[1,2,10,11] In this approach, surface wrinkles are formed in a bilayer material system consisting of a stiff thin film supported on a soft elastic substrate upon induction of an interface area mismatch of the film with respect to the substrate. Strategies employing both passive and active substrates have been used to achieve and regulate the deformation required to induce thin film buckling. Strategies with passive materials often involve the release of a temporarily stretched substrate, such

[a] Department of Biomedical & Chemical Engineering, Syracuse University, Syracuse, NY 13244, USA. E-mail: jhhender@syr.edu
[b] BioInspired Syracuse: Institute for Material and Living Systems, Syracuse University, Syracuse, NY 13244, USA
[c] Center for Biotechnology and Interdisciplinary Studies, Rensselaer Polytechnic Institute, Troy, NY 12180, USA
[d] Department of Chemical and Biological Engineering, Rensselaer Polytechnic Institute, Troy, NY 12180, USA

† Electronic supplementary information (ESI) available. See DOI: https://doi.org/10.1039/d4tb00112e

as polydimethylsiloxane (PDMS).[1,2,10,11] With this approach, the passive material must be mechanically stretched at constant strain while the thin film is applied so that subsequent release and contraction of the substrate creates compressive stress to induce thin film buckling.[11,12] Without the presence of the external force, the maintenance of a desired strain in passive elastomers is not feasible.[12] Due to this limitation, it is often difficult or impractical to conduct mechanically-actuated buckling in physiologically relevant environments, such as cell culture or *in vivo*.

To overcome this drawback, active substrates can be used to induce surface wrinkling. In particular, surface wrinkling has been studied extensively on shape-memory polymers (SMPs),[11–14] which are smart polymeric materials that can undergo on-demand shape change without the presence of an external force.[12,15] The on-demand shape change is achieved *via* SMPs' capacity to be programmed from a permanent shape to a temporary shape and then later revert to the permanent shape upon exposure to an external stimulus (*e.g.*, change in temperature, pH, or magnetic field).[16–18] Prior studies on wrinkling on SMPs have included a cytocompatible SMP bilayer system in which wrinkles formed in a gold thin film due to uniaxial contraction of an SMP substrate when warmed to body temperature.[14] The wrinkles displayed feature sizes on the micrometer and sub-micrometer scale. Using this system, we have studied static and dynamic topographical effects on cell alignment,[14] orientation of the Golgi body relative to the nucleus,[19] superdiffusivity in cell motility,[20] myofibril reorganization of human cardiomyocytes,[13] and the dynamic profile of cardiomyocyte focal adhesions.[21] In addition to the use of shape memory, shrinking or swelling of the film is another active mechanism that can be similarly used to study or leverage wrinkling.[1,2,10,11] For example, Chen *et al.*[22] fabricated a wrinkled substrate from polyethylene films that underwent thermal shrinkage to generate aligned wrinkles. Using this wrinkled substrate, the functional alignment of human embryonic stem cell derived cardiomyocytes were studied. Zhao *et al.* created surface wrinkles on non-adhesive hydrogel films by swelling in water, without implementing any template or specialized facilities. The presence of the wrinkling pattern enabled the self-assembly of mesenchymal stem cells.[23]

Although progress has been made in understanding the effects of wrinkle topographies on cellular behavior, wrinkling on active materials has largely been limited to bilayer systems with a thin metal or synthetic polymeric[13,14] film coated on the active material. When considering biomedical applications, surface wrinkles fabricated using thin metallic films lack transparency, preventing imaging by transmitted light microscopy and limiting to reflective modes the films' use in optic and photonic devices. Metal surfaces are also not biologically relevant or bioactive and can elicit a foreign body reaction when implanted *in vivo*.[11,12,24] When considering the complex architectures of devices such as stents or porous tissue engineering scaffolds, it is also relevant that the techniques available for depositing metal films as well as many synthetic polymer films can be limited in their ability to uniformly coat complex surfaces and porous structures and can present toxicity risks associated with metallic reaction products or solvents.[24–28] Further, surface wrinkles fabricated using synthetic polymers often do not facilitate cell adhesion without additional surface functionalization.[3,13]

Biopolymer films, including chitosan, polydopamine, and silk fibroin (SF),[29–32] have the potential to address many of the limitations of metal or synthetic polymer films and thereby provide new options for generating surface wrinkles on the surfaces of active materials. Unlike metal films, biopolymer films are relatively transparent and can possess innate or tailorable bioactivity.[29–31] Generally being aqueously soluble, many biopolymers can also be deposited uniformly on complex surfaces or throughout porous structures through processes that include spin coating,[32] dip coating,[33,34] and molecular self-assembly.[25]

Despite the potential for biopolymer wrinkling on active materials to advance the materials science of wrinkling, surface functionalization of active materials, and fields in which both wrinkles and active materials are being employed or studied, study of biopolymer wrinkling on active materials has to date been limited. Wang *et al.*[31] produced oriented polydopamine (PDA) wrinkles on polydopamine/polystyrene, with the compressive strain triggered by a large change in temperature that leveraged the difference in thermal expansion coefficients of the substrate and polydopamine, and studied the effect of varying PDA thickness on the wrinkling properties (*e.g.*, wavelength, amplitude). In work from a different team, Wang *et al.*[32] created silk wrinkled patterns by designing a bilayer system that consisted of a soft PDMS substrate spin coated with a stiff SF thin film and, again using a mismatch in thermal expansion coefficients, demonstrated wrinkle patterns useful for information encoding devices. Thus, these and related studies demonstrated the feasibility wrinkling biopolymers on passive substrates under non-hydrated conditions and the potential of the wrinkles in non-biological applications.

Due to the limited work to date, several important questions remain, including the following: (1) whether wrinkling of a biopolymer on an active material, such as an SMP, is possible and, specifically, whether a sufficient mismatch in the plane-strain modulus of a biopolymer film and the plane-strain modulus of an active substrate can be produced to achieve a critical strain in the range producible by the active material; (2) the extent to which the amplitude and wavelength produced by wrinkling would agree with current buckling theory as well as observations from metallic and synthetic polymer thin film wrinkling on active materials; (3) the extent to which biopolymer secondary structure would influence wrinkling and wrinkle stability when dry and when hydrated, and the converse effect of those factors on secondary structure; (4) and the extent to which hydration state would affect the formation, amplitude, and wavelength of biopolymer wrinkles.

To address these questions and as a step toward broadly establishing strategies for biopolymer wrinkling on active materials, here we studied wrinkling of SF films on SMPs under both dry and hydrated (simulated cell culture) conditions. We developed an active, dynamic bilayer wrinkling system by coating a thermo-responsive SMP substrate with a SF thin film.

Upon heat-induced contraction, the SF-SMP bilayer induces wrinkle formation in the SF. We characterized wrinkle topography using optical and atomic force microscopy to examine the effects of SMP programmed strain magnitude and recovery temperature, SF processing variables, and aqueous media on the stability, morphology, and silk network secondary structure of the protein-based topography. We studied cytocompatibility using C3H/10T1/2 mouse embryonic fibroblast cells, and we characterized wrinkles produced when triggering of the SF-SMP was performed under hydrated conditions.

2. Experimental section

2.1. Shape-memory polymer (SMP) substrate preparation

Commercially available semicrystalline thermoplastic polyurethane (TPU) pellets (MM-4520; SMP Technologies, Inc., Japan) with a nominal glass transition temperature (T_g) of 45 °C were purchased. According to the manufacturer's technical sheet, the TPU comprises hard segments of 4,4′-diphenylmethane diisocyanate and soft segments of polypropylene glycol and polyethylene glycol. Prior to sample fabrication, the SMP pellets were dried for 12 h at 50 °C in a vacuum oven to remove any residual moisture. To create hot-pressed SMP substrates, sample fabrication was conducted by adapting a previously published fabrication procedure.[35] Briefly, pellets (20 g) were placed sandwiched between two Teflon sheets (to improve surface smoothness) with a 0.40 mm thick metal spacer. Using a benchtop hydraulic press (Carver 3851-0, USA), the pellets were preheated to 200 °C for 1 h and then compressed at 1 ton for 5 min. Tap cold water was used to cool the top and bottom platens prior to releasing the compressive force and removing the samples. The resultant film was sectioned into 50 mm by 5 mm rectangular strips. To program the strain that would subsequently be recovered during shape-memory activation, each rectangular SMP strip was preheated in an isothermal oven at 50 °C for 5 min then stretched uniaxially to one of four tensile strain magnitudes (25, 45, 65, and 300%) using a custom screw-driven manual stretcher[36] and cooled in a freezer at −20 °C for 10 min to fix the stretched, temporary shape. Once fixed, samples were removed from the stretcher and stored in a desiccator until use.

2.2. Thermal characterization

To characterize thermal degradation of the SMP, thermal gravimetric analysis (TGA) was conducted using a Q500 (TA Instruments., DE, USA). Samples (n = 3, 5–10 mg) were placed in platinum pans (Fisher Scientific., MA, USA) and heated to 600 °C at 10 °C min^{-1}. As previously described,[37] a differential scanning calorimeter (DSC) Q200 (TA Instruments., DE, USA) was used to measure the glass transition temperatures of the SMP. Briefly, samples (n = 3, 3–5 mg) were placed in T-zero aluminum pans (TA Instruments., DE, USA), equilibrated at −40 °C, heated to 250 °C at 20 °C min^{-1}, kept isothermal for 2 min, cooled to −40 °C, kept isothermal for 2 min, and finally reheated to 250 °C at a rate of 20 °C min^{-1}. The dry T_g was calculated during the second heating cycle as the midpoint of the inflection using the Glass/Step Transition function on the TA Universal Analysis software (v. 4.5A, TA Instruments, DE, USA). To measure wet T_g, samples (n = 3) were incubated at 37 °C in deionized water for 24 h, pressed dry, and placed in T-zero aluminum pans with hermetic lids (TA Instruments, DE, USA). A single heating cycle to 160 °C at 10 °C min^{-1} was performed, and the wet T_g was calculated as the midpoint of the inflection using the glass/step transition function on the TA Universal Analysis software.

2.3. Silk fibroin (SF) preparation

Each SMP substrate was coated with a SF thin film, which would subsequently buckle into a wrinkled state to form the silk wrinkles during SMP shape recovery. Prior to use, a commercially available stock solution of SF (~100 kDa, extracted from the Bombyx Mori silkworm, Ca# 5154, Advanced Biomatrix., CA, USA) was centrifuged at 3700 rcf for 30 min to remove any protein aggregates. The 5% w/v stock solution was stored in a −80 °C freezer prior to use. To coat the SMP substrates with SF, each substrate was placed onto double-sided tape on a glass slide, which was then mounted and secured on a WS-650-23B spin coater (Laurell Technologies Corporation., PA, USA). To determine the effect of thickness on the silk wrinkle morphology, the SMP was spin-coated with SF at 1500 or 3000 rpm for 1 min. Secondary structures produced from regenerated SF consist of random coils, β-turns, and α-helices, which usually exist in amorphous domains, and β-sheets, which usually exist in crystalline domains. Alcohol treatment or water annealing can easily an increase in β-sheet content, which is a conversion that is frequently employed for biomaterial applications.[25,33,34] The SF-SMP samples were then stored in a vacuum desiccator to dry overnight. To determine the effect of alcohol-treatment-duration on secondary structural alteration from random coil and/or helix structure to β-sheet structure and to minimize water solubility, the SF-SMP bilayer samples were post-treated in a solution of 70% methanol (v/v) at different time points (30, 40, 50, and 60 min) prior to SMP recovery. The treated samples were stored in a desiccator to dry overnight.

2.4. Spectroscopic analysis

To characterize the silk network, Fourier transform infrared (FTIR) spectroscopy (Nicolet i70 Spectrometer, Fisher Scientific., MA, USA) was performed on SF films at a resolution of 0.4 cm^{-1} over 128 scans between wavenumber range of 600–4000 cm^{-1}. The strained SF-SMP samples (ε = 45%) were analyzed before and after methanol treatment, with unmodified SMP substrate as a control. The samples were also analyzed following shape recovery. As a structural protein, SF can potentially undergo molecular conformational transition when exposed not only to methanol but also to mechanical deformation.[38] Silk wrinkles are formed when the SMP of the SF-SMP bilayer system is subjected to uniaxial compression. To better understand the effect of this mechanical loading during silk wrinkle formation (*i.e.*, after shape recovery), the changes in the secondary structures of the silk network were studied at 40 °C and 70 °C by using second derivative deconvolution and multi-peak fitting analysis of the amide I region of the

FTIR spectra as described by Yang *et al.*[39] The secondary structures (random coil, β-sheet, α-helix, β-turn) in the silk network were determined by deconvoluting the amide I region (1600–1700 cm^{-1}) of the FTIR signal using the multipeak fitting package in IgorPro8 (WaveMetrics Inc. OR, USA). First, the contribution of the SMP substrate was removed from the SF-SMP spectra using a multiple linear regression formula. Here a multiplicative and vertical shift factor were determined using residual sum of squares (RSS) to superimpose the SF-SMP and SMP-only spectra over the region of 1720–1760 cm^{-1}. This region was chosen because SF has no contribution within this range, thus all of the signal in this region can be attributed to the SMP substrate. The two determined shift factors were applied to the SMP-only spectra, then the SMP-only spectra were subtracted from the unmodified SF-SMP spectra. Then for the background-subtracted SF-SMP spectra, the number and initial location of peaks in the amide I region were determined by assigning peak locations to the local minima of the second derivative of the spectra. A linear baseline was applied to the endpoints of the original spectra before loading the peaks into the software. The peaks were all assigned as Gaussian with identical widths and heights; peak locations, widths, and heights were all allowed to iterate until the multipeak fitting solver converged to a solution. Peak assignment for SF is based on work by Lammel *et al.*[40] Adsorption bands within the ranges of 1610–1635 cm^{-1} and 1695–1700 cm^{-1} were attributed to β-sheet structures, adsorption bands within 1666–1695 cm^{-1} were attributed to β-turn structures, whereas the random coil and α-helical structures were combined into one adsorption band range of 1635–1666 cm^{-1}. The adsorption band range 1600–1610 cm^{-1} is termed "other," as this region represents protein aggregates and tyrosine contributions.[41] Three independent replicates were measured for each condition (n = 3). Total secondary structure percentages were determined by summing the area of all fitted peaks within the aforementioned specified ranges, then divided by the total area under the curve.

2.5. Characterization of wrinkles under dry conditions

To study wrinkling of SF films under dry conditions, the strained SF-SMP samples were placed in an isothermal oven at 40 °C or 70 °C for 30 min to trigger return of the SMP to its original permanent shape (Fig. 1).

Two temperatures were studied because non-cytocompatible SMP-based wrinkle systems have previously been tuned not only by varying the film thickness or programming strain but also by varying the temperature used during the shape recovery process.[11] The specific range was selected because, without the plasticizing effect of hydration, it was anticipated that complete recovery would occur at a temperature between 40 °C and 70 °C. Following triggering, the presence of the silk wrinkle morphology was confirmed by imaging with a KH-8700 optical digital microscope (Hirox, Japan) at different magnifications (350×, 700×, 1750×, and 3500×). To characterize the silk wrinkle morphology, a Nano R-2 CA atomic force microscope (AFM; Pacific Nanotechnology, USA) was used in contact mode with a Si_3N_4 cantilever (spring constant: 5 N m^{-1}). A 50 μm square area was scanned with a scan rate of 1.5 Hz. The wrinkle wavelength and amplitude were determined using Nanoscope Analysis software (Bruker, Massachusetts, USA). Silk film thickness

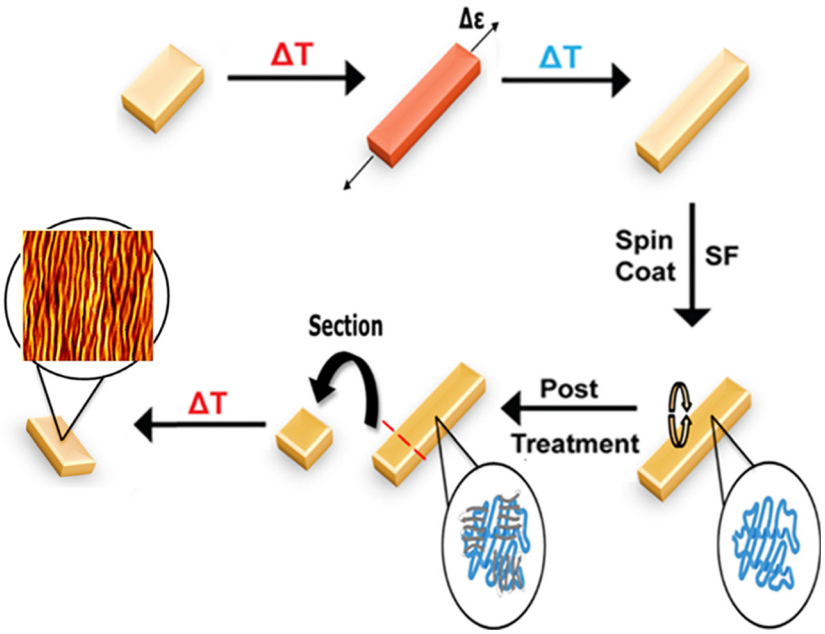

Fig. 1 Silk wrinkle formation overview. The thermo-responsive shape memory polymer (SMP) is heated above its glass transition temperature, stretched uniaxially, and then cooled to remain fixed in a temporary, stretched shape. The SMP is spin-coated with silk fibroin (SF) and then post-treated with methanol to induce a conformational transition from random coil to β-sheet structure in the silk network. To induce shape recovery, the SMP is heated to recover to the original shape. Heat-induced shrinkage of the SMP enables the SF coating to buckle, which induces the formation of silk wrinkles on the surface. The representative atomic force microscopy (AFM) micrograph shown is that of a 25% strained SF-SMP following SMP recovery.

was determined using AFM. A scratch-and-scan method was performed in which a part of the SF film was removed by scratching it with a razor blade. The scratched area was scanned in contact mode and the scan rate was fixed to 1.5 Hz on a 50 μm square area. The film thickness was determined by calculating the step-height between the film and bare substrate on the AFM micrograph.

2.6. Characterization of silk wrinkle stability in media

To study stability of wrinkled SF films in simulated cell-culture conditions (aqueous media at body temperature), SF was spin-coated onto 25%, 45%, and 65% pre-strained SMPs at 1500 rpm and 3000 rpm. Prior to characterization, samples were immersed in 200 μL of complete medium: Basal Medium Eagle (BME) supplemented with 10% fetal bovine serum (FBS), 1% penicillin/streptomycin (PS), and 1% L-glutamine (L-glut) for 24 h. Optical microscopy was used to confirm the presence of the wrinkled surfaces before and after immersion in media, and AFM was used to characterize the amplitude and wavelength prior to and following media incubation.

2.7. Cytocompatibility of silk wrinkles

Cytocompatibility of the engineered silk wrinkled structures was evaluated using C3H10T1/2 mouse embryonic fibroblasts (ATCC, Virginia, USA). Strained SMPs coated at 1500 rpm with SF and post-treated in methanol, unstrained SF-SMPs coated at 1500 rpm and post-treated in methanol, and unstrained SMPs not coated with SF were sterilized using UV light for 30 min in a biosafety cabinet (BSC) prior to cell seeding. Cells were cultured in a T75 flask with complete medium at 37 °C/5% CO_2. Once 70% confluency was achieved, cells were dissociated with 0.025% trypsin for 5 min, centrifuged at 160 rcf for 5 min, resuspended with complete medium, droplet seeded onto each sample in a 96 well plate with a density of 4500 cells per well and 150 μL of complete medium, and incubated at 37 °C, 5% CO_2 for 24 h. To evaluate sample cytocompatibility, live (Calcein AM, green) and dead (Ethidium Homodimer-1, red) stains (Invitrogen, IL, USA) were applied to the cell-seeded samples for 30 min at 37 °C prior to fluorescent imaging under an Axiovert inverted fluorescence microscope (Zeiss Microscopy, Germany). Three fields of view were imaged per sample, and cytocompatibility testing was performed on three independent samples at three different times. Cell viability was calculated by dividing the number of live cells by the total number of cells.

2.8. Characterization of silk wrinkle formation in media (wet recovery)

To study wrinkling of SF films in simulated cell-culture conditions (aqueous media at body temperature), SMPs were strained to 300% to achieve a pronounce shape recovery (or contraction) to induce buckling of the SF film in media. Selection of the 300% programmed strain magnitude was informed by preliminary experiments, which indicated that high strain was required to achieve buckling of the film to a wrinkled state following wet recovery, presumably due to plasticization of the silk by water and the accompanying reduction in the modulus of the silk film. The strained samples were then spin-coated with SF, and post-treated in methanol to prevent dissolution of the silk film. To conduct wet recovery, samples (n = 3) were sectioned into 0.3 cm^2 rectangles, UV sterilized for 30 min in a BSC, and placed in a 48 well plate with 200 μL of complete medium. Samples were placed in a 28 °C incubator for 2 h and then transferred to a 37 °C incubator to trigger SMP recovery. After 24 h, samples were rinsed with deionized water to prevent the formation of salt crystals on the surface of the wrinkles upon drying. To verify the presence of the silk wrinkle morphology, samples were imaged in brightfield before and after wet recovery using the brightfield channel on the Axiovert microscope. The silk wrinkle morphology and wrinkle characteristics were also characterized by AFM, as previously described for dry wrinkle characterization.

2.9. Statistical analysis

Results are reported as mean ± standard deviation. All experiments were repeated three times (n = 3). One-way ANOVA

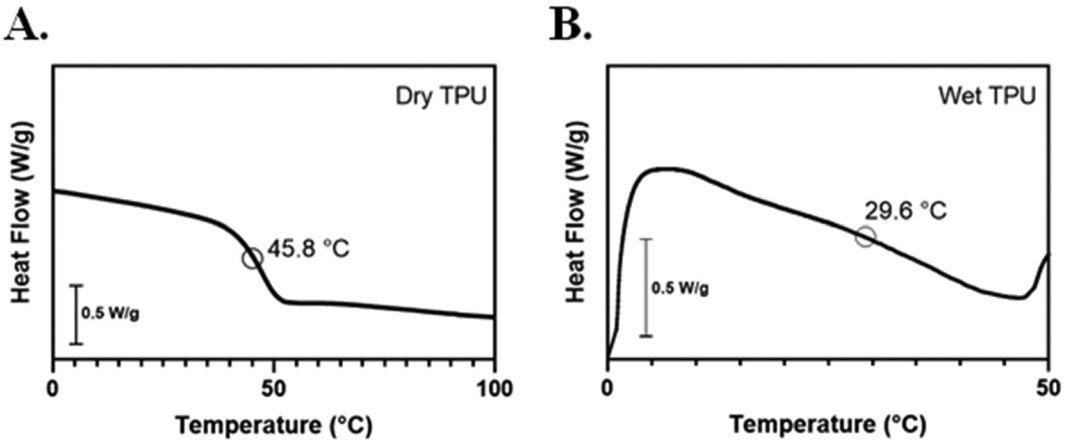

Fig. 2 Thermal characterization revealed that the glass transition temperature (T_g) of the thermoplastic polyurethane (TPU) decreased when hydrated. Differential scanning calorimetry (DSC) curves following second heating cycle of (A) dry and first heating cycle of (B) wet shape memory MM-4520 thermoplastic polyurethane.

followed by Holm Sidak's multiple comparisons tests between groups was performed for comparisons involving more than two groups. Student's *t*-test was used for two-group comparisons. The significance of results is reported as $*p < 0.05$, $**p < 0.01$, $***p < 0.001$, $****p < 0.0001$.

3. Results and discussion

3.1. SMP thermal properties

Dry and wet glass transition temperatures of the MM-4520 SMP were determined by DSC. Based on the DSC thermographs (Fig. 2), the dry T_g was 45.8 °C, which is comparable to that reported by the manufacturer.[37] Following hydration, we observed a reduction in T_g to 29.6 °C. We attribute the decrease in T_g to moisture having a plasticization effect on the urethane bonds of the TPU, with weakening of hydrogen bonding interactions in the polymer network causing the reduction in T_g. This finding is consistent with previous studies demonstrating the effect of moisture on the T_g of these commercially available shape-memory polyurethanes.[37,42] Since the TPU is a T_g-based SMP, we can deduce that hydration served to plasticize the polymer matrix, inducing a drastic decrease in T_g This indicates why the T_g of the substrate in the dry state was designed to slightly exceed body temperature (37 °C) to prevent premature recovery.

3.2. Dry wrinkle characterization

SF is a natural fibrous protein derived from the cocoons of domesticated *Bombyx mori* silkworms that has been widely used as a thin film to modify the surface properties of polymeric substrates and devices to optimize or control cell behavior, enhance biocompatibility, provide desired mechanical properties suitable for biomedical applications, and elicit a lower inflammatory response than other common polymers, such as polylactic acid and collagen.[25,43,44] Here we found that, upon SMP recovery, the microscopic change in surface topography induced a macroscopic change in the opacity of the SMP surface indicating successful silk wrinkle formation (Fig. 3).

Using AFM, we observed a range of wrinkle wavelengths and amplitudes as a function of the SMP pre-strain and SF spin coating speeds. When the SMP underwent shape recovery at 70 °C (Fig. 4(A)), wrinkle amplitude and wrinkle wavelength increased as SMP pre-strain increased for both spin coating speeds.

Specifically, for 3000 rpm, wavelength increased from 1.5 ± 0.02 to 2.7 ± 0.2 μm with an increase in SMP pre-strain (Fig. 4(B)). The amplitude increased from 241 ± 12.5 to 423 ± 22.4 nm with an increase in SMP pre-strain (Fig. 4(C)). Similar results were observed for the spin coating speed of 1500 rpm, for which wavelength increased from 2.5 ± 0.3 to 4.6 ± 0.007 μm as SMP pre-strain increased (Fig. 4(D)) and amplitude increased from 423 ± 16.3 to 770 ± 48.3 nm (Fig. 4(E)). Additionally, decreasing wrinkle wavelength (Fig. S1, ESI†) and wrinkle amplitude (Fig. S1, ESI†) was observed with increasing spin-coating speed for all pre-strains.

To confirm the formation of the silk wrinkled surface patterns near body temperature, the SMP underwent shape recovery at 40 °C. Based on the AFM micrographs, different silk wrinkled morphologies along with different wavelengths and amplitudes were acquired (Fig. 5(A)) compared to the wrinkle topographies obtained following recovery at 70 °C. The quantitative results still demonstrated that the wrinkle wavelength

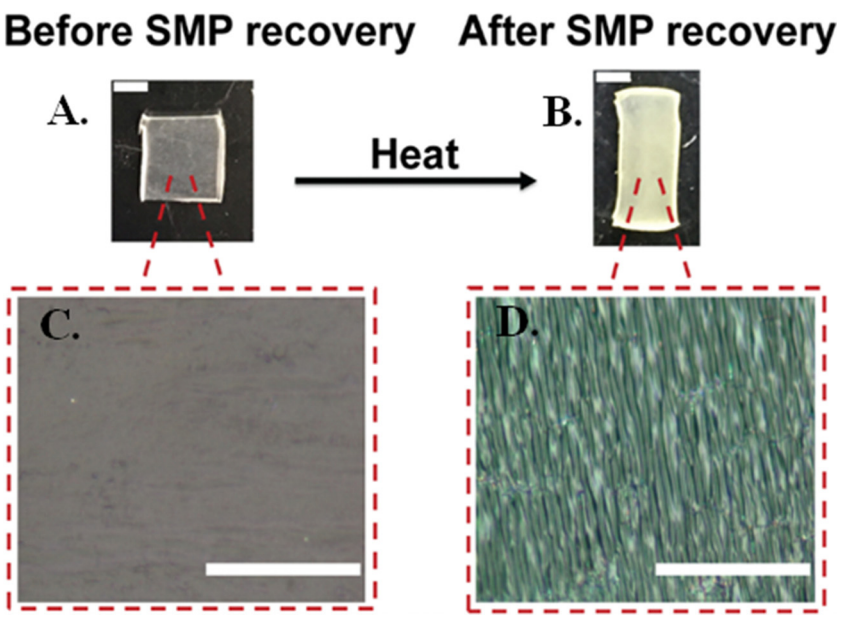

Fig. 3 Macroscopic change in opacity of the shape memory polymer (SMP) surface induced a microscopic wrinkle formation following shape recovery. (A) Photo of 45% pre-strained SMP spin-coated with silk fibroin (SF) at 3000 rpm and then treated in methanol solution before and (B) after SMP recovery (scale bars = 5 mm). (C) Optical micrograph of 45% pre-strained SMP coated with SF and treated with methanol before and (D) after SMP recovery (scale bars = 20 μm).

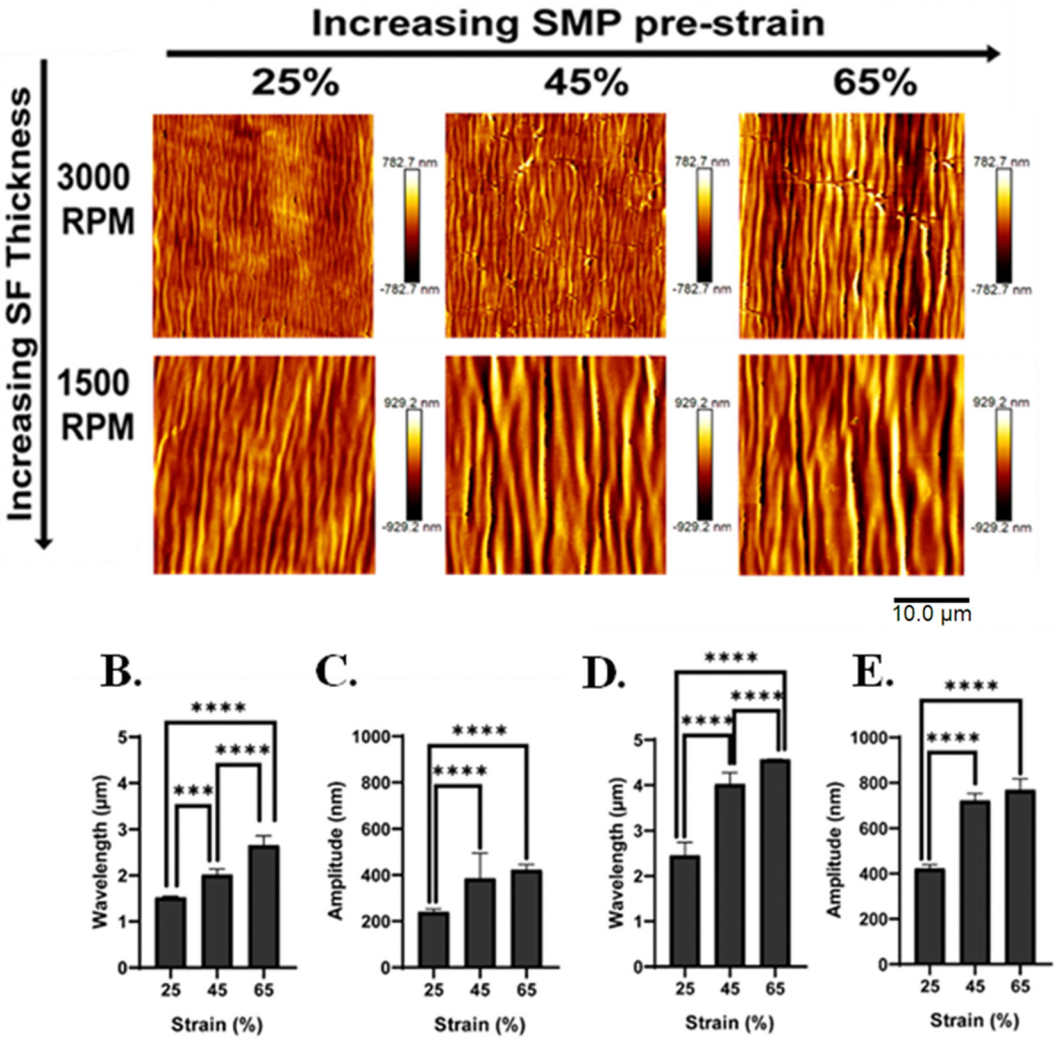

Fig. 4 Regardless of film thickness, silk wrinkle amplitude and wrinkle wavelength increased with increasing SMP pre-strain at a 70 °C recovery temperature. (A) Atomic force microscopy images of the silk wrinkled topographies recovered at 70 °C with different spin-coating speeds. Scale bar = 10 μm. Detailed characterization of the effects of SMP pre-strain on wrinkle wavelength and amplitude for spin-coating speeds of (B and C) 3000 rpm and (D) and (E) 1500 rpm. (n = 3, one-way ANOVA, followed by Holm Sidak's multiple comparisons test between groups, *$p < 0.05$, **$p < 0.01$, ***$p < 0.001$, ****$p < 0.0001$).

and amplitude increased as the SMP pre-strain increased for both spin-coating speeds. For 3000 rpm, the wrinkle wavelength increased from 2.0 ± 0.2 to 3.2 ± 0.2 μm with increasing SMP pre-strain (Fig. 5(B)), and the amplitude increased from 276 ± 56.5 to 579 ± 79.4 nm with an increase in SMP pre-strain (Fig. 5(C)). These trends were similarly observed for 1500 rpm, in which the wavelength increased from 2.5 ± 0.1 to 4.3 ± 0.2 μm as the SMP pre-strain increased (Fig. 5(D)), and the amplitude increased from 402 ± 23.2 to 743 ± 76.5 nm (Fig. 5(E)). Furthermore, similar to the wrinkle characteristics at 70 °C, there was also a decrease in the wrinkle wavelength (Fig. S2, ESI†) and amplitude (Fig. S2, ESI†) as the spin-coating speed increased for all pre-strains.

Collectively, these results demonstrate an increase in wrinkle wavelength and amplitude with decreasing spin-coating speed, which is due to an increase in coating thickness. When conducting the spin coating technique, the thickness of the deposited film can be modulated by the solution viscosity and the spin-coating speed. This study focused on modulating the thickness of the SF film by decreasing the spin-coating speed during spin coating which leads to an increase in film thickness.[45] We observed with a high spin-coating speed of 3000 rpm, the thickness of the SF film was 145 nm (measured *via* AFM), while with a low spin-coating speed of 1500 rpm, the thickness of the SF increased to 250 nm.

Returning to the question of the extent to which the amplitudes and wavelengths produced by silk wrinkling would agree with the current buckling theory as well as observations from previous metallic and synthetic polymer thin film wrinkling data: our findings represented both consistent and contrasting findings when compared to the theory and/or previous reports. Based on the bilayer buckling theory reported by Chang *et al.*,[46] the relationship for wavelength, amplitude, and critical strain required to create wrinkles for small deformation is given as

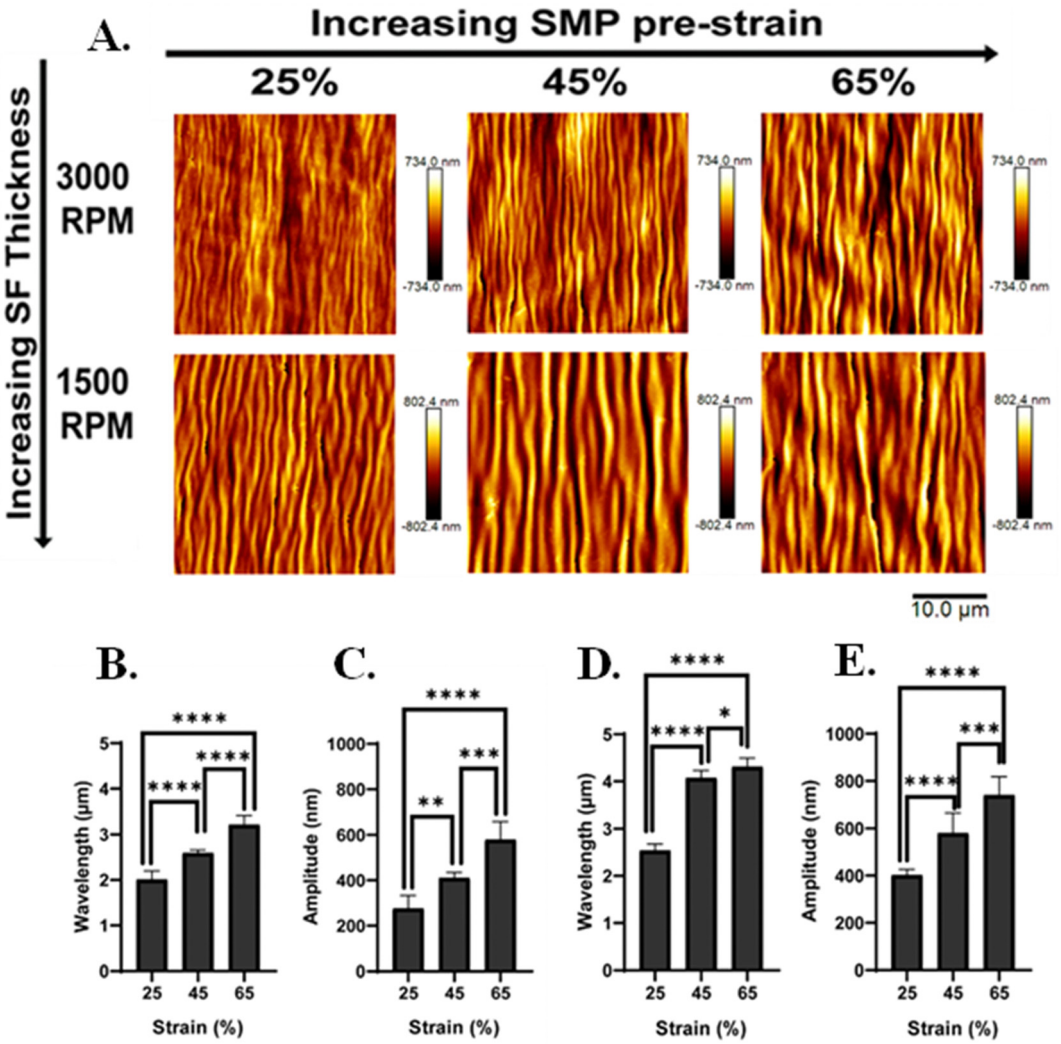

Fig. 5 Regardless of film thickness, silk wrinkle amplitude and wrinkle wavelength increased with increasing SMP-pre-strain at a 40 °C recovery temperature, as had also been observed at 70 °C (Fig. 4). (A) Atomic force microscopy images of the silk wrinkled topographies recovered at 40 °C with different spin-coating speeds. Scale bar is 10 μm. Detailed characterization of the effects of SMP pre-strain of on the wrinkle topographies with a spin-coating speed of (B) and (C) 3000 rpm and (D) and (E) 1500 rpm. (n = 3, one-way ANOVA, followed by Holm Sidak's multiple comparisons test between groups, *$p < 0.05$, **$p < 0.01$, ***$p < 0.001$, ****$p < 0.0001$).

followed:

$$\lambda = 2\pi h_f \left(\frac{\bar{E}_f}{3\bar{E}_s}\right)^{\frac{1}{3}} \quad (1)$$

$$A = h_f \left(\frac{\varepsilon}{\varepsilon_c} - 1\right)^{\frac{1}{2}} \quad (2)$$

$$\varepsilon_c = \frac{1}{4}\left(\frac{3\bar{E}_s}{\bar{E}_f}\right)^{\frac{2}{3}} \quad (3)$$

where λ is the wavelength, h_f is the film thickness, $\bar{E}_f$ is the plane-strain modulus of the film, $\bar{E}_s$ is the plane-strain modulus of the substrate, A is the amplitude, ε is the applied compressive strain, and ε_c is the critical strain (minimum strain) needed to induce buckling. The relationship between the spin-coating speed and silk wrinkle characteristics observed in our results (Fig. S1 and S2, ESI†) indicate that as the thickness of the SF film increase due to decreasing spin-coating speed, the wrinkle wavelength increases, in agreement with eqn (1) of the bilayer buckling theory and as has been observed in prior thin film wrinkling studies.[11,12] While, in agreement with eqn (2), the wrinkle amplitude also increases, with increasing film thickness due to decreasing spin-coating speed. Additionally, we found that amplitude increases with increasing SMP programmed strain, in agreement with eqn (2) of the bilayer buckling theory and as has been reported in previous thin film wrinkling work.[11,12]

In terms of contrasting results, we observed that the wavelength increased with increasing SMP pre-strain. Interestingly, this result contrasts with our previous study,[14] in which the gold-SMP bilayer system demonstrated a decrease in wrinkle wavelength with increasing programmed strain. Similarly, Schauer *et al.*[11] developed an all-polymer wrinkling bilayer

system and found that, with increasing pre-strain, the resulting wrinkle wavelength decreased approximately linearly. However, it is worth noting that Chang *et al.*[46] investigated the effect of strain *rates* on the wrinkle characteristics of tunable PDMS-wrinkled films. They observed that wrinkle amplitude increased with increasing strain rate, but no general trends were observed in terms of the wrinkle wavelength, suggesting that strain may have little or no influence on wavelength. Additionally, Chung *et al.*[47] fabricated anisotropic micro-wrinkled surfaces by mechanical compression of an ultraviolet-ozone-treated PDMS elastomer and found that the wrinkle wavelength does not change, but the wrinkle amplitude follows a square-root dependence with strain.

Furthermore, with our SF-SMP wrinkle system, the silk wrinkle topographies are not only tunable by varying the spin-coating speed or programming strain but by varying the recovery temperature applied to induce triggering during the shape recovery process. In particular, different trigger temperatures can cause different rates of recovery for the SMP, which may explain the unexpected trend with wavelength *vs.* temperature. In addition, we would expect the rate of shape recovery to affect silk secondary structure, which will also affect the properties of the SF film, including mechanical properties (examined by Fourier Transform Infrared Spectroscopy, Section 3.3). According to eqn (1), the wrinkle wavelength also depends on the plane-strain modulus, which for a polymer or biopolymer can have a strong dependence on temperature. The reported elastic moduli of the MM-4520 SMP at 45 °C and 70 °C were 0.14 GPa and 0.002 GPa, respectively,[48] the reported plane-strain modulus of silk was 2.14 GPa,[32] and the reported Poisson's ratio of the SMP (ν = 0.4).[49] In the present study, we can, therefore, anticipate a decrease in SMP plane-strain modulus with both increase in temperature and with hydration. Having observed little or no change in wavelength with increasing temperature, the buckling theory would suggest that the silk modulus may be undergoing proportional decreases in modulus with increasing temperature.

Thus, although several findings we observed are consistent with theory and prior studies, the results suggest that temperature may have affected the observed trends in wavelength and amplitudes. Whether this effect, when considered in terms of the modulation of the SMP and silk modulus, would be consistent with the current theory, is unclear. While the effect of temperature of the SMP has been reported, the effect of temperature on the mechanical properties of silk fibroin remains less well understood. We consider that issue an intriguing question raised by this study and one worth pursuit, but beyond the scope of the current study.

Lastly, we also observed that cracks formed upon recovery at a 70 °C recovery temperature (Fig. 4(A)). Specifically, this occurred for the surface patterns fabricated with a 3000 rpm spin-coating speed at higher SMP pre-strain. Previously, we discovered[14] discovered an increase in crack formation with an increase in SMP pre-strain. For the silk bilayer platform, crack formation is more dependent on the recovery temperature and film thickness than the pre-strain, and we would anticipate that crack formation could be mitigated at high strains by regulating the recovery kinetics. Although crack formation is associated with plastic deformation, delamination, which would arise if there was complete failure of the interface between the film and substrate, was not observed in our platform prior to or during cell culture.

3.3. Secondary structure analysis by Fourier transform infrared (FTIR) spectroscopy

3.3.1. Effect of varying methanol treatment time on secondary structures in SF. FTIR confirms that a conformational transition from random coil/α-helix to β-sheet structure occurred and that SF became rich in β-sheets following MeOH treatment. The FTIR spectra of the uncoated SMP shows characteristic bands of the urethane groups at ~3200 cm^{-1} (bonded N–H stretching) and ~1703 cm^{-1} (bonded C═O stretching; Fig. 6(A)).

Information regarding the secondary structures present in SF can be analyzed using the amide I band (1700–1600 cm^{-1}), which corresponds to the absorption of the peptide backbone. To determine secondary structure content, the bare SMP FTIR signal was first subtracted from each spectrum, and then deconvolution of the amide I band with (Fig. S4–S7, S8, ESI†) and without (Fig. S3 and S8, ESI†) MeOH treatment was performed. Without MeOH treatment, the spectra of SF-SMP exhibits an absorption peak at ~1650 cm^{-1} in the amide I region, corresponding to random coils/α-helix (Fig. 6(A)). In contrast, absorption at ~1624 cm^{-1} is observed for all MeOH-treated groups (Fig. 6(B)), suggesting a conformational transition to β-sheet structure following MeOH treatment. Such transition to a β-sheet rich structure is typically necessary for the formation of a water-insoluble silk material that can be used in cell culture applications.

3.3.2. Effect of shape memory uniaxial contraction on SF secondary structures. By analyzing the FTIR spectra of SF films with and without substrate shape change (Fig. S9–S14, ESI†), buckling was found to affect SF secondary structure. At 40 °C (Fig. 7(A)), we observed that the unstrained SF-SMP with no MeOH treatment had a β-sheet content of 4.9% ± 1.7 and random coil/α-helix content of 74.3% ± 6.6. However, the strained SF-SMP with no MeOH treatment showed a significant increase in the overall β-sheet content to 16.2% ± 2.9 and decrease in the overall random coil/α-helix content to 54.7% ± 10.1 as compared with the unstrained SF-SMP with no MeOH treatment. This indicates that mechanical deformation of the SMP substrate alone can cause conformational changes within the SF film and increase β-sheet content. Additionally, the strained SF-SMP with MeOH treatment showed a significant increase in the overall β-sheet content to 29.8% ± 1.1 as compared with the strained SF-SMP with no MeOH treatment. The additional exposure to MeOH for the strained SF-SMP provides a greater increase in the overall β-sheet content as compared with the strained SF-SMP that has no exposure to MeOH, confirming that alcohol treatment can also cause SF to undergo conformational transition in our system.

In contrast, when the SF-SMP was heated to 70 °C for shape memory recovery (Fig. 7(B)), there was no significant difference

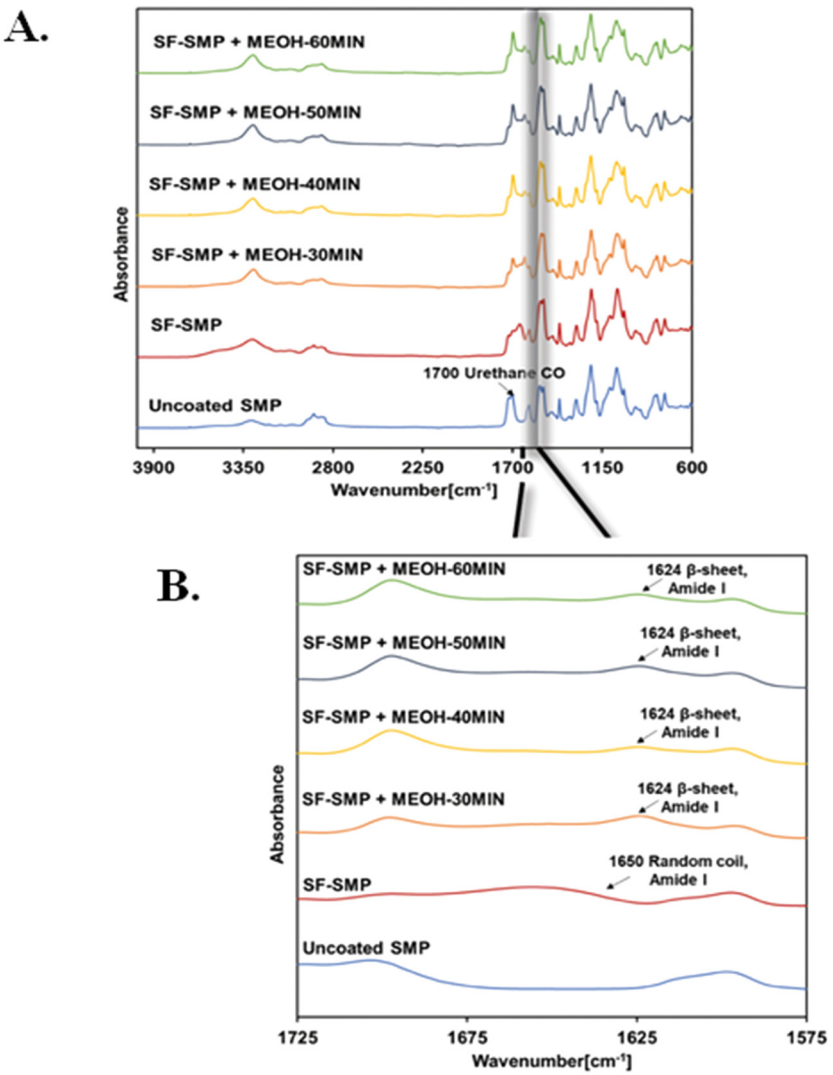

Fig. 6 Fourier transform infrared spectroscopy (FTIR) spectra confirmed the presence of silk fibroin (SF) on the surface of the shape memory polymer (SMP) and successful secondary conformational changes in the silk network after methanol (MeOH) treatment. (A) Full scale FTIR spectra of SF-SMP (brown line) and SF-SMP with MeOH treatment at different treatment times of 30 min (orange), 40 min (yellow), 50 min (dark blue), and 60 min (green). (B) Expanded FTIR spectra indicates a conformational transition from random coil/α-helix (before MeOH treatment) to β-sheet structure (after MeOH treatment) in the peptide backbone infrared region for amide I (1700–1600 cm^{-1}).

(p = 0.3340) in the overall β-sheet content between the unstrained SF-SMP with no MeOH treatment and the strained SF-SMP with no MeOH treatment. Thus, uniaxial contraction of the SMP at 70 °C had no apparent effect on β-sheet content. We can speculate that, since the shape recovery temperature affects the rate of uniaxial contraction of the SMP, the rate of contraction could impact how the SF undergoes conformational changes. For example, with a higher recovery temperature (70 °C), the SMP substrate undergoes a faster shape recovery. Although silk wrinkle formation is achieved, the faster rate of strain recovery may not allow sufficient time for changes in chain conformation. In contrast, with a lower recovery temperature (40 °C), the SMP will undergo a slower uniaxial contraction. Here silk wrinkles are also formed, but the slower rate of strain recovery may allow SF chains sufficient time to rearrange at the molecular level. These results indicate shape-memory-actuated wrinkling of SF films can induce β-sheet formation. This finding is consistent with a previous report of mechanical loading affecting secondary structures, in which tensile stress applied to *B. mori* regenerated SF films *via* uniaxial drawing and produced progression from randomly oriented chains to aligned β-sheets in the film.[38]

In the present study, the deformation of the SF film is more complex than simple tension, as uniaxial contraction of the SMP substrate can be expected to produce both compression (in the direction of contraction) and tension due to the Poisson effect (in the perpendicular direction). Moreover, it has been reported that the in-plane stress in thin-films following wrinkle formation is non-uniform in the bilayer material system. Specifically, the crests of the surface wrinkles are dominated by compressive stresses near the film-substrate interface but can convert into tensile stresses near the free surface after a critical value of wrinkle curvature is exceeded.[50] Thus, in the present

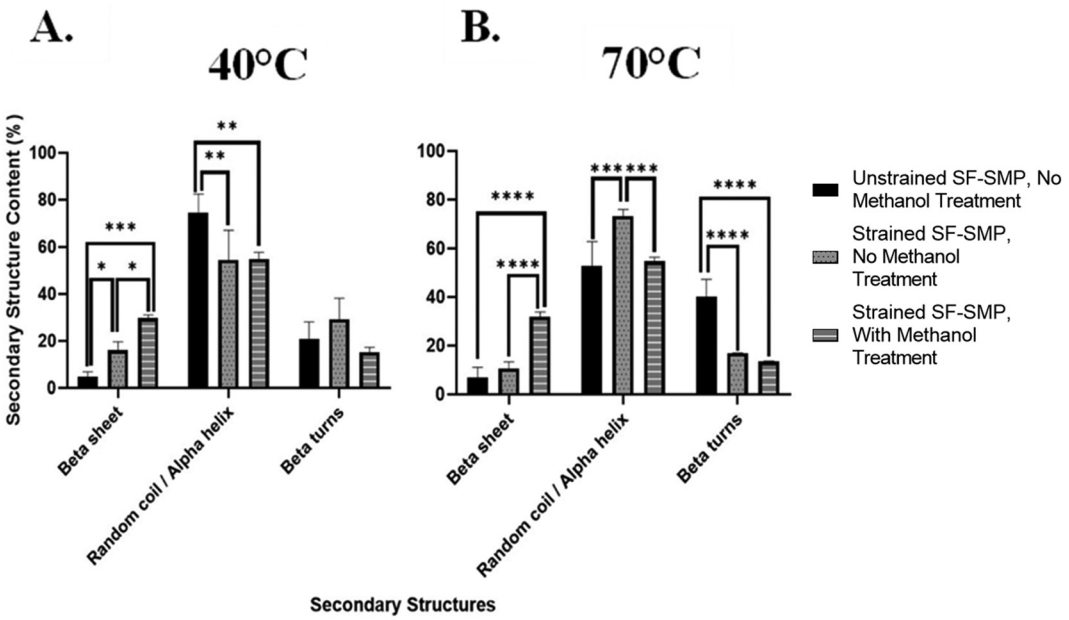

Fig. 7 Shape memory polymer (SMP) uniaxial contraction provides secondary structural changes in the silk network and induces β-sheet formation. (A) Detailed comparison of the secondary structure content following SMP shape recovery SF-SMP at 40 °C. (B) Detailed comparison of the secondary structure content following SMP shape recovery at 70 °C. (n = 3, one-way ANOVA, followed by Holm Sidak's multiple comparisons test between groups, *$p < 0.05$, **$p < 0.01$, ***$p < 0.001$, ****$p < 0.0001$).

work, the results from the uniaxially contracting samples raise the question of whether compression, tension, or a combination of loading modes is inducing β-sheet formation in the silk network of the wrinkling SF-SMP bilayer. To better understand whether the observed mechanical effects on silk secondary structure are due to compression, tension, or a combination of loading modes, we employed samples programmed for biaxial contraction (ESI,† Methods I and III) and bending actuated tensile expansion (ESI,† Methods II and III) to study SF thin film secondary structure under loading more uniform than that of uniaxial contraction.

3.3.3. Effect of shape memory biaxial compression on secondary structures in silk network. To determine if compressive stress serves as the driving force to induce β-sheet formation in the silk network, we fabricated a pure compressive SMP substrate that undergoes only biaxial compression without any tensile stress. Here uniform contraction with equal magnitudes were applied concurrently in both the x- and the y-directions following shape recovery of the SMP (or during silk wrinkle formation). The effect of this mechanical loading on the secondary structures in SF were again studied at 40 °C and 70 °C using multi-peak fitting analysis of the FTIR spectra (Fig. S15–S20, ESI†). At 40 °C (Fig. 8(A)) and 70 °C (Fig. 8(B)), our results depicted how compressive forces has little-to-no effect (not counting the effect of MeOH exposure to our strained SF-SMP) on inducing β-sheet formation nor contributes to any molecular conformational changes in the silk network.

3.3.4. Effect of shape memory bending actuated tension on secondary structures in silk network. To determine if tensile stress serves as the driving force to induce β-sheet formation in the silk network, we fabricated an SMP substrate that undergoes bending actuation. As the SMP undergoes shape recovery (or bending), the polymeric fibers in the lower region of the substrate were dominated by tensile stresses. The upper and lower regions of the substrate experience an immense amount of stress during bending actuation, especially whichever is of a more important distance from the neutral axis of the substrate. The effect of this bending actuated tension on the secondary structures in SF were investigated at 40 °C and 70 °C using multi-peak fitting analysis of the FTIR spectra (Fig. S21–S26, ESI†). At 40 °C (Fig. 9(A)), the unstrained SF-SMP with no MeOH treatment had a β-sheet content of 4.4% ± 1.1 and random coil/α-helix content of 75.7% ± 3.6. While the strained SF-SMP with no MeOH treatment had a slight increase in the overall β-sheet content to 10.0% ± 1.0 and a significant decrease in the overall random coil/α-helix content to 67.6% ± 3.1 as compared with the unstrained SF-SMP with no MeOH treatment.

This was further observed at 70 °C (Fig. 9(B)), in which the unstrained SF-SMP with no MeOH treatment had a β-sheet content of 11.5% ± 2.0 and random coil/α-helix content of 69.3% ± 3.4. On the other hand, the strained SF-SMP with no MeOH treatment also had a slight increase in the overall β-sheet content to 16.4% ± 2.4 and a significant decrease in the overall random coil/α-helix content to 52.9% ± 3.5 as compared with the unstrained SF-SMP with no MeOH treatment. Although there was no significant difference of the overall β-sheet content at 40 °C (p = 0.0979) and 70 °C (p = 0.1723) between the unstrained and strained samples with no exposure to MeOH, we still believe that tensile stresses are the driving force to induce secondary structural changes in the silk network. This is because we observed a significant difference of

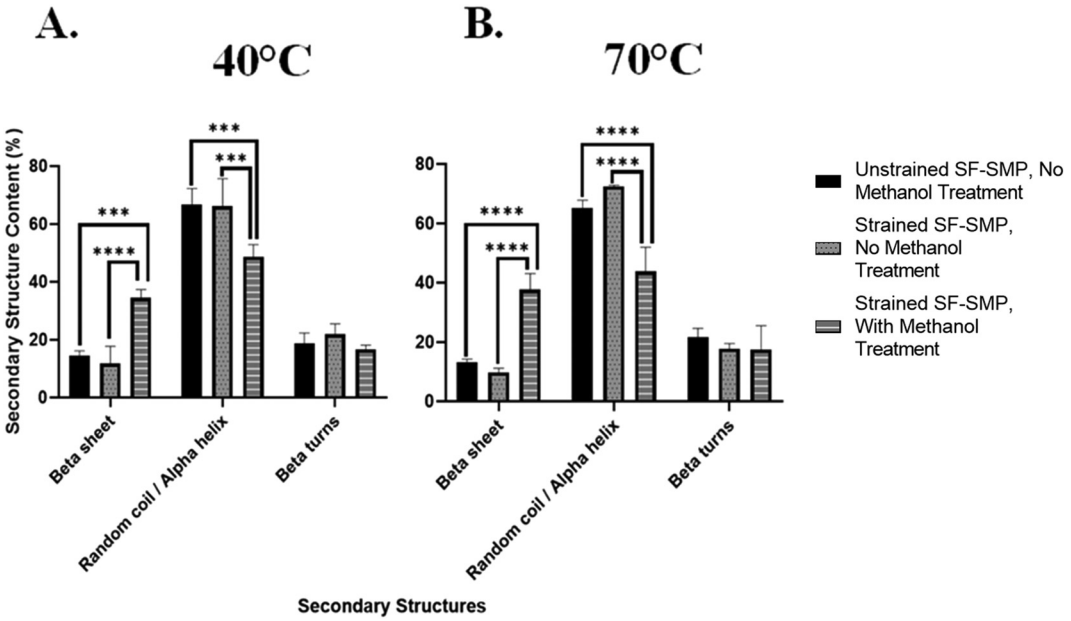

Fig. 8 Shape memory polymer (SMP) biaxial contraction provides no effect on secondary structural changes in the silk network and does not induce β-sheet formation. (A) Detailed comparison of the secondary structure content following SMP shape recovery SF-SMP at 40 °C. (B) Detailed comparison of the secondary structure content following SMP shape recovery at 70 °C. (n = 3, one-way ANOVA, followed by Holm Sidak's multiple comparisons test between groups, *$p < 0.05$, **$p < 0.01$, ***$p < 0.001$, ****$p < 0.0001$).

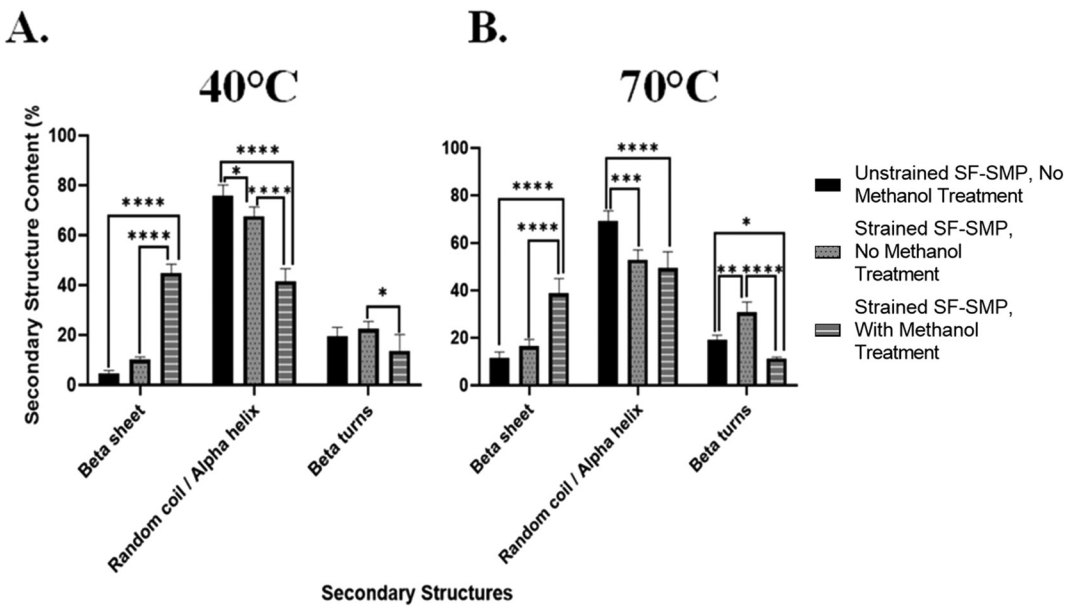

Fig. 9 Shape memory polymer (SMP) bending actuated tension can provide to structural changes in the silk network. (A) Detailed comparison of the secondary structure content following SMP shape recovery SF-SMP at 40 °C. (B) Detailed comparison of the secondary structure content following SMP shape recovery at 70 °C. (n = 3, one-way ANOVA, followed by Holm Sidak's multiple comparisons test between groups, *$p < 0.05$, **$p < 0.01$, ***$p < 0.001$, ****$p < 0.0001$).

the overall random coil/α-helix content at 40 °C (p = 0.0208) and 70 °C (p = 0.0003) between the unstrained and strained groups with no MeOH treatment. We can deduce that tension forces primarily contribute to β-sheet formation in the chains of the protein. Additionally, this is further supported in the literature, in which Huot *et al.*[38] studied the effect of tensile stress on the secondary structures of regenerated SF films. They reported that either step-by-step or continuous stretching and/or tension induces gradual β-sheet formation which is oriented along the chain. This aligns with our finding on how SMP bending actuated tensile stresses could contribute to secondary structural changes in the SF film.

Additionally, since we observed a significant difference of the overall β-sheet content at both 40 °C and 70 °C between the strained SF-SMP with no MeOH treatment and the strained SF-SMP with MeOH treatment, we were interested in understanding if the combination of the MeOH and strain provides a greater effect on β-sheet formation compared to just MeOH (an unstrained SF-SMP with MeOH exposure-Fig. S27, ESI†) or if the entire effect is solely from MeOH. Deconvolution of the amide I band for the unstrained SF-SMP with MeOH treatment was also conducted with multi-peak fitting analysis (Fig. S28 and S29, ESI†). Surprisingly, at both 40 °C and 70 °C, the overall β-sheet content was slightly higher for the unstrained SF-SMP with MeOH treatment as compared with the strained SF-SMP with MeOH treatment. Although there was no significant difference between the two sample groups, we speculate that since the application of SF film was conducted *via* dip coating, there could be potential variance in the uniformity of the coating that could affect the distribution of the secondary structure throughout the surface of the SMP. Moreover, due to the greater volume of solvent used during dip coating, thicker films will require longer drying times.[51] Hence, the increased drying time increases the likelihood for the deposited coating to begin to run before it completely dries, ultimately leading to an uneven film distribution that could affect how the secondary structures orient themselves in the silk network. Additionally, we observed that the β-sheet content in the control samples (unstrained SF-SMP, without any MEOH treatment) varies across the different mechanical loading experiments. To achieve a particular mechanical deformation (*e.g.*, uniaxial contraction, biaxial compression, and bending actuated tension), a certain substrate geometry had to be fabricated. Since different substrate geometries were used for each mechanical loading experiment, we speculate that the substrate geometry could also influence the uniformity of the silk coating following deposition, which could introduce variations in β-sheet content due to differences in drying times or other variables.

Thus, following spectroscopic analysis, our overall findings are: (1) MeOH treatment generates high β-sheet content regardless of application of strain or shape recovery temperature. If MeOH is applied, the effect of strain is not observable within error caused by the heterogeneities present in the sample; (2) for non-MeOH treated samples, which have relatively lower β-sheet content, the β-sheet content is slightly increased by uniaxial contraction but not by biaxial contraction. This effect only occurs noticeably for the lower recovery temperature. Though not statistically significant, bending tension results suggest that this increase in β-sheet content is due to tension. Ultimately, based on the collective results, we speculate the mechanical effects on SF secondary structure observed in the uniaxial contraction samples is likely due primarily to Poisson effect expansion (tension) perpendicular to the direction of uniaxial contractile recovery. This further suggests that manipulating the loading conditions for the bulk substrate in our bilayer system can affect the secondary structures in the silk network regardless of any complex, small scale stresses taking place inside the SF film.

3.4. Silk wrinkles stability in media

Although prior work demonstrated the feasibility of using silk as a thin film in bilayer wrinkling systems intended for use in different environments,[32] it did not explore the effects of SF topographical surfaces under physiologically relevant conditions, such as when hydrated and at body temperature, or on cellular responses, and to date silk wrinkles remain unstudied in cell culture or biomedical applications. To evaluate the stability and pattern of the wrinkle morphology in an aqueous environment, the films were soaked in complete medium at 37 °C for 24 h and imaged by AFM. Due to hydration, the silk wrinkles dissipated for all samples prepared with a 3000 rpm spin-coating speed (data not shown). We speculate that a higher speed deposited less material on the surface of the SMP, ultimately leading to small silk wrinkle amplitudes that did not have enough volume of silk to remain stable in the aqueous environment. In contrast, the silk wrinkles remained present for all samples prepared with a 1500 rpm spin-coating speed (Fig. 10(A)). With soaking, the wavelength of the pre-strained silk wrinkles increased, and the amplitude decreased (Fig. 10(B)). These results indicated the wavelength of the wrinkles increased due to spreading out by hydration of the SF film, but the hydration ceased prior to completion.

Additionally, when considering the plane-strain modulus in eqn (1) of the bilayer buckling theory, the wrinkle wavelength is also dependent on the plane-strain modulus, which for a polymer or biopolymer can be affected by hydration. The reported elastic modulus of the MM-4520 SMP when hydrated and at 25 °C is 70.4 MPa,[37] and the reported elastic modulus of silk when hydrated is 18.70 MPa.[52] Although values for the plane-strain modulus of hydrated silk fibroin are currently not reported in the literature, the plane-strain modulus of the biopolymer would be expected to show a similar decrease from the reported 2.14 GPa noted in Section 3.2. In the present study we can, therefore, anticipate a decrease in SMP plane-strain modulus with hydration. Having observed an increase in wavelength following media incubation, theory would suggest that the SMP experienced a greater decrease in modulus with hydration than did the silk or that the observed results are not consistent with theory.

Although our findings suggest that the hydration state may affect the observed trends in the wrinkle wavelength and wrinkle amplitude, whether this effect, when considered in terms of the modulation of the SMP and silk modulus, would be consistent with the current theory, is unclear. While the effect of hydration on the modulus of the SMP has been reported, the effect of hydration on the mechanical properties (*e.g.*, plane-strain modulus) of silk remain less well understood. We consider this an additional interesting question worth future study.

Moreover, our results can be further attributed to how water induces property changes in polymers. In the biomaterials field, water has been demonstrated to induce changes in the molecular structure of many hydrophilic polymers; ultimately affecting the physical properties of polymeric materials.[53] In particular, water has been reported to influence both the amorphous and crystallite domains of SF. For the amorphous domains of silk, water plays the role as a plasticizer, which

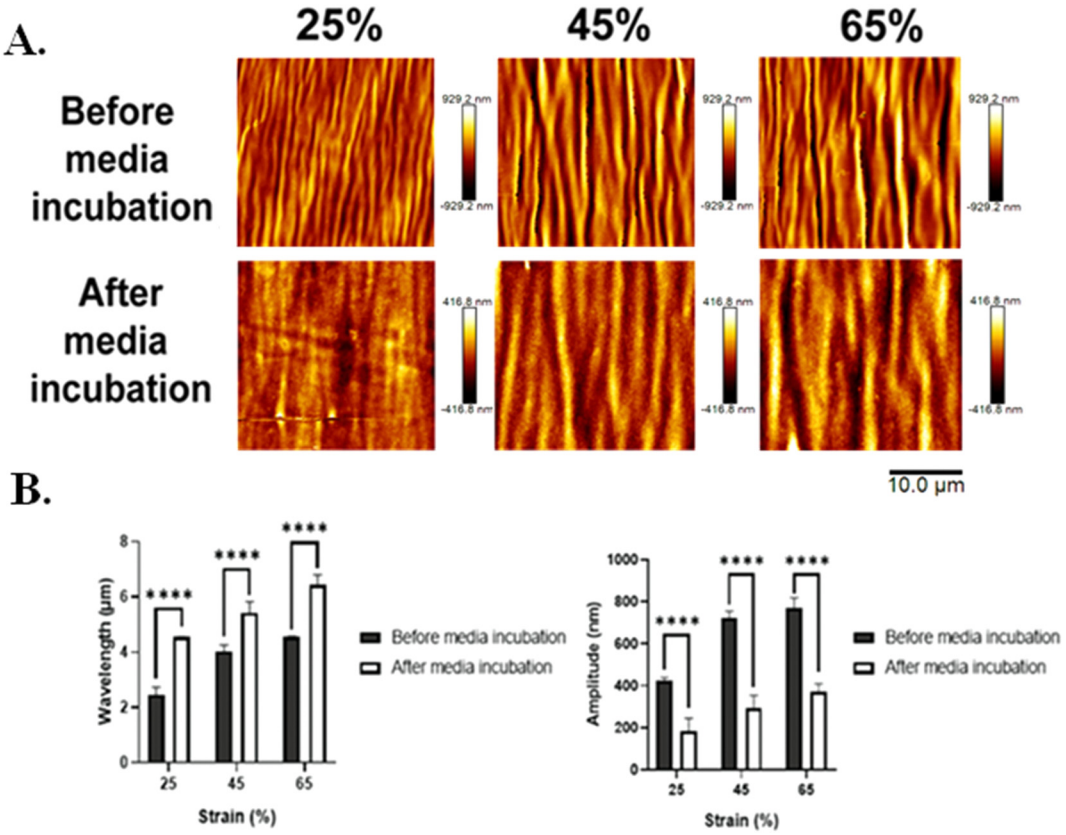

Fig. 10 Silk wrinkle amplitude decreased, while the wrinkle wavelength increased following media incubation. (A) Atomic force microscopy images of the silk wrinkled topographies prepared *via* a spin-coating speed of 1500 rpm before and after immersion in media. Scale bar is 10 μm. (B) Detailed characterization of the wrinkle topographies following immersion in media for 24 h. (n = 3, Student's t-test for two group comparisons, *$p < 0.05$, **$p < 0.01$, ***$p < 0.001$, ****$p < 0.0001$).

helps to enhance chain mobility in the amorphous region and reduces brittleness of SF.[53] However, for the β-sheet crystallite domains of silk, which primarily dictates the strength of silk, Cheng *et al.* used molecule dynamics simulation on a β-sheet crystallite of *Bombyx mori* silk and determined that water weakens the strength of the β-sheet crystallite.[54] Specifically, they reported that water molecules play a weakening role in the formation of hydrogen bonds between β-chains, ultimately reducing the stability of the β-sheet crystallite.[54] This understanding regarding the effect of water in the silk network provides context on how the silk wrinkles are susceptible to molecular changes that could affect its stability and morphology when hydrated.

3.5. Cytocompatible silk wrinkles

To assess cytocompatibility of the silk wrinkles, C3H/10T1/2 cells were cultured on the silk wrinkled structures (coated at 1500 rpm due to persistence of wrinkled topography in media) along with an unstrained SF-SMP (unwrinkled) and uncoated SMP to serve as controls. Cells were able to attach to and spread on the wrinkled surface (Fig. 11(A)). Although cellular viability was high on the controls, the engineered silk wrinkled structures displayed 99.8% cell viability (Fig. 11(B)), suggesting the silk wrinkle topographies' potential to serve as a cell culture platform. Additionally, more cells were attached to the wrinkled surface (Fig. 11(C)) as compared to the flat SF-SMP and uncoated SMP. The present results complement recent progress in implementing SF for cell culture applications. Cell adhesion is crucial in cell communication and regulation and serves as fundamental importance in the development and maintenance of tissues for tissue engineering.[55–57] However, weak cell attachment to silk surfaces has been reported in the past. For example, cells cultured on silk films and hydrogels can often display a spherical morphology and generate microaggregates, because cell–cell anchorage dominates cell–matrix interactions.[58] The cell-spheroids are poorly bound to silk surfaces and can simply be released upon low mechanical forces.[58] Similarly, Zhang *et al.* cultured pig iliac endothelial cells on *B.mori* SF films or nano-fibrous scaffolds. It was observed that the cells adhered approximately 40% better to fibrous matrices.[59] According to our results, the silk wrinkles serving as efficient topographical cues could be responsible for good cell adhesion compared to the flat silk controls.

Additionally, prior studies have demonstrated that substrates with topography dimensions similar to the cell size range or smaller lead to the establishment of stable cell-surface attachment.[60] In the case of wrinkled topographies, cell adhesion is enhanced by wrinkles with wavelengths and amplitudes

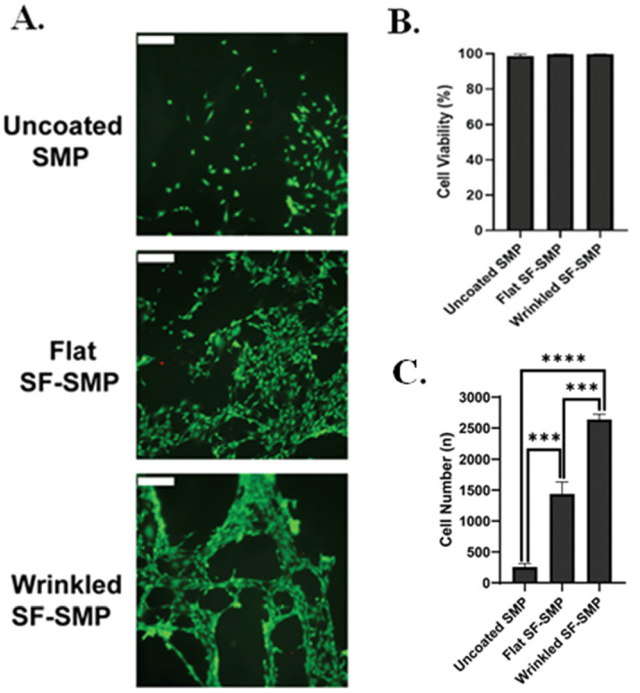

Fig. 11 Silk wrinkles displayed high cell viability and adhesion. (A) Representative fluorescent images of live (green) and dead (red) C3H/10T1/2 cells after 24 h for uncoated shape memory polymer (SMP), flat SF-SMP, and wrinkled SF-SMP. (B) Quantitative results of cell viability and (C) cell number of calculated attach cells (n = 3) samples, with three areas images per sample, one-way ANOVA, followed by Holm Sidak's multiple comparisons test between groups. Scale bar = 100 μm.

of this scale.[61] Previous studies have shown that the size of the wrinkled structures can guide the formation of focal adhesion complexes.[62,63] Yang *et al.*[62] fabricated polydimethylsiloxane substrates with anisotropic wrinkle topographies with various wavelengths and amplitudes to investigate their influence on the behavior of human bone marrow-derived mesenchymal stem cells. By using immunofluorescence staining for the focal adhesion protein vinculin, they found that wrinkled surfaces with smaller wavelengths (0.5 μm and 3 μm) enhanced the expression of vinculin compared to flat surfaces and wrinkled surfaces with larger wavelengths (10 μm and 27 μm).[62] The area of the focal adhesion complexes for the stem cells were also characterized, and they observed that the focal adhesion area for cells cultured on wrinkled structures with smaller wavelengths were larger than those of flat surfaces and wrinkled structures with larger wavelengths.[62] Hence, compared to flat surfaces and wrinkled surfaces with larger wavelengths, wrinkled surfaces with smaller wavelengths contribute to facilitating the formation of focal adhesion complexes.

Lastly, many studies have demonstrated that cells can be oriented (or align) on wrinkled surfaces. Although in our cytocompatibility assays, the cells did not show obvious cell alignment, this was not the focus of our experiment and further studies can be conducted to investigate the effect of the silk wrinkle characteristics on cell orientation. We can speculate that cell alignment was not observed qualitatively because the cell density was not conducive to cell alignment. We believe the seeding density chosen for the experiment was too high to allow conclusions regarding a mechanobiologically-driven alignment response. In future studies, a lower cell seeding density could be used to achieve a culture of isolated cells that are dominated by cell-material contact and minimal cell–cell contact to improve an alignment effect. For the present study, we focused on viability and adhesion, but the interaction of mammalian cell orientation with the silk wrinkled surfaces is an interesting area for future study due to the varied wavelengths and amplitudes that could be used to study or control mammalian mechanobiology. However, additional study would be required to determine the extent to which these wrinkles promote a mechanobiological response.

3.6. Silk wrinkles recovered in media (wet recovery)

Silk wrinkle formation in the hydrated state (aqueous media) was investigated to determine the extent to which the SF-SMP bilayer system is stable at 28 °C (a cell-compatible temperature below body temperature at which devices could be held if wrinkling is not yet desired) and the extent to which the system would fully recover at 37 °C (body temperature, a clinically relevant temperature for use in on-demand wrinkling). Here we observed no wrinkle formation when samples were kept in media at 28 °C for 2 h (Fig. 12(A) and (C)), but silk wrinkles were found to form under simulated cell culture conditions when the incubation temperature was elevated to 37 °C (Fig. 12(B) and (D)), driven by bulk recovery of the SMP substrate at 37 °C when hydrated. We also observed a significant difference in the wrinkle wavelength (Fig. 12(E)) and amplitude (Fig. 12(F)) of the bilayer system before and after SMP recovery. Additionally, the wrinkle characteristics of the silk wrinkles formed in the wet state (Fig. 12) differed from the wrinkles formed in the dry state (Fig. 4 and 5). Specifically, in the wet state, the wrinkle wavelength and amplitude were significantly reduced compared to those observed in the dry state. Lastly, we did not observe delamination between the SF film and SMP substrate, either during wrinkle formation or cell culture, indicating a robust interface without an additional adhesive interlayer sometimes required in bilayer platforms.[64–66]

Further, it is important to emphasize that both the TPU and silk film of our system is susceptible to interaction with water. As previously mentioned, the shape memory TPU yields a T_g of 45.8 °C (dry), which is lowered to 30.7 °C once hydrated due to water plasticization. Garces *et al.*[37] reported that the same shape memory MM-4520 TPU experiences a rapid modulus dropped as immersion time in water increases. This further indicates that, due to plasticization, hydration will have a substantial effect on the mechanical properties of the SMP. Regarding how hydration influences silk, Lawrence *et al.*[52] investigated the effects of hydration on SF film material properties for MeOH-treated films. That work revealed that film swelling increases when films are placed in a hydrated environment, and this is most likely due to water absorption inducing changes in the protein's secondary structures.[52] It was also found that hydrated silk films demonstrate a decrease in

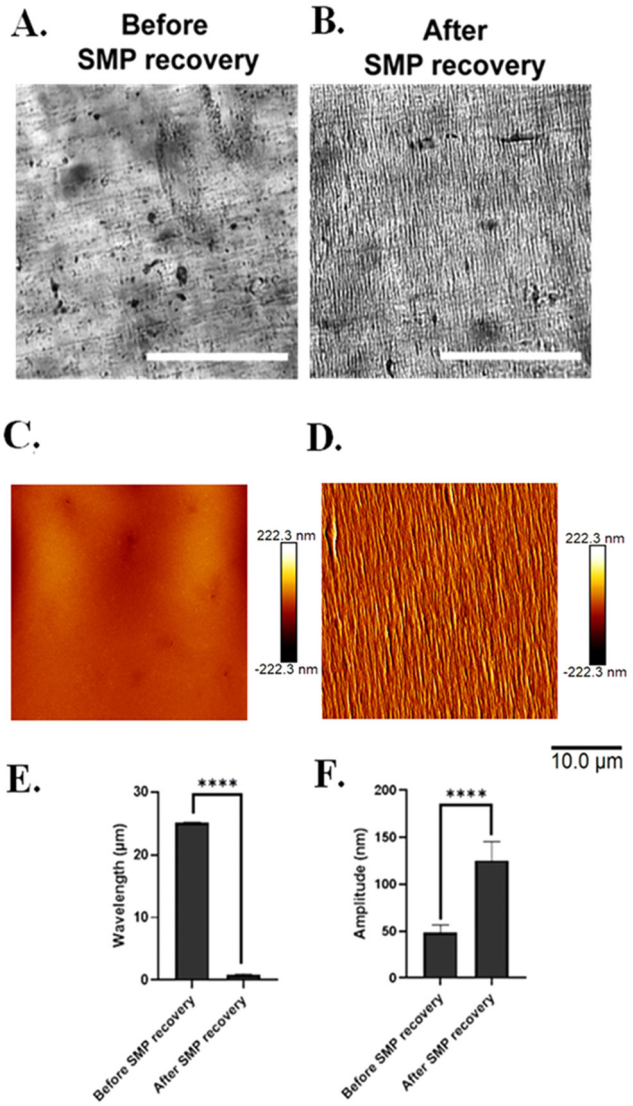

Fig. 12 Successful silk wrinkle formation under cell culture conditions. Representative brightfield images of an active 300% pre-strained wrinkled sample (A) before wet shape memory polymer (SMP) recovery and (B) after wet SMP recovery. Scale bar = 100 μm. Atomic force microscopy images of the active pre-strained wrinkled sample. (C) before and (D) after wet SMP recovery. Scale bar = 10 μm. Detailed characterization of the (E) wrinkle wavelength and (F) amplitude before and after SMP recovery. (n = 3, Student's t-test for two group comparisons, *$p < 0.05$, **$p < 0.01$, ***$p < 0.001$, ****$p < 0.0001$).

modulus when compared to dry films, further indicating that the presence of water has a significant influence on the mechanical properties of silk film regardless of β-sheet content.[52]

Moreover, since this was a proof-of-concept study, we did not characterize the kinetics of bulk material recovery as the SMP recovers in aqueous conditions. Garces *et al.*[37] also revealed how hydration can have a significant influence on the shape recovery performance of the TPU. Specifically, the ability for the material to reach full recovery and the recovery rate decreased following immersion in water.[37] They speculated that this behavior is due to plastic deformation in which the chains in the polymer network suffer from the decrease of the T_g and the programmed strain. Based on previous studies and our findings on how plasticization affects various properties of the SMP, analysis of the recovery kinetics behavior and its contribution to silk wrinkle formation as the materials undergoes wet recovery will be further explored in future experimentation. Since hydration also affects material properties of silk, we also believe characterizing the time course of wrinkle formation during wet recovery in future studies would be advantageous towards employing this dynamic topography on a time scale possibly slower than, similar to, or faster than that of cell division and reorganization which could provide new insight into cell behavior and mechanobiology.

Hence, our overall findings from this proof-of-concept of study can inform strategies for studying cell–material interactions in a dynamic environment. Although major advances in the biomaterials field have enabled the study of cell–material interactions using material systems with varying degrees of complexity (*e.g.*, topography, tunable elasticity), most studies have been restricted to static material systems that do not mimic the *in vivo* dynamic environment.[55–57] *In vivo*, dynamic changes in the ECM can elicit specific cellular phenotypes and behaviors during tissue development, repair, and disease initiation and progression.[56,67] Thus, there remains a need to develop material systems with enhanced complexities that can undergo dynamic alterations in properties (*e.g.*, topography, surface chemistry) under cytocompatible conditions. To address this need, we and others have developed SMP platforms with the capacity to undergo dynamic topographical changes with the presence of cells. Neuss *et al.* was the first to report *in vitro* SMP actuation (or shape change) effects on cells. However, cells were not viable on this SMP due to shape change taking place at 54 °C.[68] We developed SMP platforms with the capacity to undergo topographic changes at 37 °C with adhered and viable cells,[69] which have been used to control and study cell mechanobiology *via* dynamic, *in situ* formation of gold wrinkles[18–20] and polyelectrolyte multilayer (PEM) wrinkles[13] and increases or decreases in alignment of electrospun fibers.[70] Soon after, Ebara *et al.* fabricated an SMP that can induce changes in the direction of topographical grooves from one direction to the orthogonal direction *in vitro* and reported that cells reorient their morphology to align with the newly formed topographical grooves.[71] Furthermore, adding to the complexity of these studies, the first 3D work fabricated an SMP hydrogel to control stem cell differentiation through changes in cytoskeletal contraction.[72] These studies have demonstrated the benefits of dynamic SMPs platforms in the study of cell mechanobiology and illustrate the potential for the wrinkling SF-SMP bilayer system of the present work to contribute to this growing field.

4. Conclusions

Here we demonstrate wrinkling of a biopolymer, SF, on an active material, an SMP, confirming that a sufficient mismatch in the plane-strain modulus of a biopolymer film and the plane-strain modulus of an active substrate can be produced to

achieve a critical strain in the range producible by the active material. The effect of SF film thickness on amplitudes and wavelengths produced by wrinkling agrees with current buckling theory as well as observations from metallic and synthetic polymer thin films. In contrast, the effect of SMP pre-strain was found to be the converse of that previously observed with wrinkling of gold films on SMP materials, possibly due to plastic determination and/or interface slips during strain loading of the SF-SMP bilayer. With respect to biopolymer secondary structure, we found that silk wrinkling increases β-sheet content, with spectroscopic analysis suggesting that the effect may be due primarily to tensile (*e.g.*, Poisson effect and high-curvature wrinkle) loading modes in the SF, despite the compressive bulk deformation (uniaxial contraction) used to produce wrinkles. Silk wrinkles fabricated from sufficiently thick films (roughly 250 nm) and formed in a dry state persist after 24 h in cell culture medium, and silk wrinkles formed in the wet state differ significantly from those formed in the dry state, with wrinkles formed in the wet state possessing much smaller wavelengths and amplitudes. The silk wrinkles also displayed high cell viability and attachment.

The cytocompatible silk wrinkles reported here demonstrate good performance as a cell culture substrate for C3H/10T1/2 cells, suggesting that the bilayer could serve as a dynamic cell culture platform in biomaterials applications, including cell mechanobiology, wound healing, and tissue engineering applications. For example, we have previously used wrinkling of a PEM film to profile the responsiveness of focal adhesions of human cardiomyocytes to a dynamic extracellular nanotopography.[21] That work was representative of much of the prior work in which wrinkles were used to study cell mechanobiology, which has generally employed synthetic (metallic or polymeric) films.[13–21,73] By establishing an approach whereby silk can be used as the film, here we broaden the potential for the wrinkle topography to be tailored to the specific mechanobiological needs of a given research inquiry. For example, SF has been used to deliver therapeutics for cancer,[74] wound healing,[74,75] and neural tissue regeneration.[74,76] The additional use of an SMP offers a unique strategy to exploit the surface topography for drug delivery applications. We anticipate that the bulk shape change could lead to an initial burst release while the SF could provide a slow, sustained release controlled by the wrinkle characteristics.[77] Due to these and other benefits, we suggest that the wrinkling SF-SMP bilayer system provides novel potential as a cell culture platform and for use in biomedical applications.

Conflicts of interest

There are no conflicts to declare.

Acknowledgements

This work was supported by the National Science Foundation's Biomaterials and Advanced Manufacturing programs (DMR-2049793 and CMMI-2022421).

References

1 A. Schweikart and A. Fery, Controlled Wrinkling as a Novel Method for the Fabrication of Patterned Surfaces, *Microchim. Acta*, 2009, **165**(3–4), 249–263, DOI: **10.1007/s00604-009-0153-3**.

2 W. Chen, X. Gui, L. Yang, H. Zhu and Z. Tang, Wrinkling of Two-Dimensional Materials: Methods, Properties and Applications, *Nanoscale Horiz.*, 2019, **4**(2), 291–320, DOI: **10.1039/C8NH00112J**.

3 R. L. Dimmock, X. Wang, Y. Fu, A. J. E. Haj and Y. Yang, Biomedical Applications of Wrinkling Polymers, *Recent Prog. Mater.*, 2020, **2**(1), 1–31, DOI: **10.21926/rpm.2001005**.

4 Z. Wang, D. Tonderys, S. E. Leggett, E. K. Williams, M. T. Kiani, R. Spitz Steinberg, Y. Qiu, I. Y. Wong and R. H. Hurt, Wrinkled, Wavelength-Tunable Graphene-Based Surface Topographies for Directing Cell Alignment and Morphology, *Carbon*, 2016, **97**, 14–24, DOI: **10.1016/j.carbon.2015.03.040**.

5 T. Wang, T. U. Luu, A. Chen, M. Khine and W. F. Liu, Topographical Modulation of Macrophage Phenotype by Shrink-Film Multi-Scale Wrinkles, *Biomater. Sci.*, 2016, **4**(6), 948–952, DOI: **10.1039/C6BM00224B**.

6 V. A. Surapaneni, M. Schindler, R. Ziege, L. C. de Faria, J. Wölfer, C. M. Bidan, F. H. Mollen, S. Amini, S. Hanna and M. N. Dean, Groovy and Gnarly: Surface Wrinkles as a Multifunctional Motif for Terrestrial and Marine Environments, *Integr. Comp. Biol.*, 2022, **62**(3), 749–761, DOI: **10.1093/icb/icac079**.

7 T. Thorsen, R. W. Roberts, F. H. Arnold and S. R. Quake, Dynamic Pattern Formation in a Vesicle-Generating Microfluidic Device, *Phys. Rev. Lett.*, 2001, **86**(18), 4163–4166, DOI: **10.1103/PhysRevLett.86.4163**.

8 D.-Y. Khang, J. A. Rogers and H. H. Lee, Mechanical Buckling: Mechanics, Metrology, and Stretchable Electronics, *Adv. Funct. Mater.*, 2009, **19**(10), 1526–1536, DOI: **10.1002/adfm.200801065**.

9 E. P. Chan, E. J. Smith, R. C. Hayward and A. J. Crosby, Surface Wrinkles for Smart Adhesion, *Adv. Mater.*, 2008, **20**(4), 711–716, DOI: **10.1002/adma.200701530**.

10 S. Yang, K. Khare and P.-C. Lin, Harnessing Surface Wrinkle Patterns in Soft Matter, *Adv. Funct. Mater.*, 2010, **20**(16), 2550–2564, DOI: **10.1002/adfm.201000034**.

11 S. Schauer, M. Worgull and H. Hölscher, Bio-Inspired Hierarchical Micro- and Nano-Wrinkles Obtained: *Via* Mechanically Directed Self-Assembly on Shape-Memory Polymers, *Soft Matter*, 2017, **13**(24), 4328–4334, DOI: **10.1039/c7sm00154a**.

12 Z. Chen, Y. Young Kim and S. Krishnaswamy, Anisotropic Wrinkle Formation on Shape Memory Polymer Substrates, *J. Appl. Phys.*, 2012, **112**(12), 1–11, DOI: **10.1063/1.4770483**.

13 S. Sun, H. Shi, S. Moore, C. Wang, A. Ash-Shakoor, P. T. Mather, J. H. Henderson and Z. Ma, Progressive Myofibril Reorganization of Human Cardiomyocytes on a Dynamic Nanotopographic Substrate, *ACS Appl. Mater. Interfaces*, 2020, **12**(19), 21450–21462, DOI: **10.1021/acsami.0c03464**.

14 P. Yang, R. M. Baker, J. H. Henderson and P. T. Mather, *In Vitro* Wrinkle Formation *via* Shape Memory Dynamically Aligns Adherent Cells, *Soft Matter*, 2013, **9**(18), 4705–4714, DOI: 10.1039/c3sm00024a.

15 J. Li, Y. An, R. Huang, H. Jiang and T. Xie, Unique Aspects of a Shape Memory Polymer as the Substrate for Surface Wrinkling, *ACS Appl. Mater. Interfaces*, 2012, **4**(2), 598–603, DOI: 10.1021/am201727a.

16 A. Lendlein, M. Behl, B. Hiebl and C. Wischke, Shape-Memory Polymers as a Technology Platform for Biomedical Applications, *Expert Rev. Med. Devices*, 2010, **7**(3), 357–379, DOI: 10.1586/erd.10.8.

17 M. Behl and A. Lendlein, Shape-Memory Polymers, *Mater. Today*, 2007, **10**(4), 20–28, DOI: 10.1016/S1369-7021(07)70047-0.

18 M. J. Haskew and J. G. Hardy, A Mini-Review of Shape-Memory Polymer-Based Materials Stimuli-Responsive Shape-Memory Polymers, *Johnson Matthey Technol. Rev.*, 2020, **64**(4), 425–442, DOI: 10.1595/205651319X15754757916993.

19 M. E. Brasch, G. Passucci, A. C. Gulvady, C. E. Turner, M. L. Manning and J. H. Henderson, Nuclear Position Relative to the Golgi Body and Nuclear Orientation Are Differentially Responsive Indicators of Cell Polarized Motility, *PLoS One*, 2019, **14**(2), e0211408, DOI: 10.1371/journal.pone.0211408.

20 G. Passucci, M. E. Brasch, J. H. Henderson, V. Zaburdaev and M. L. Manning, Identifying the Mechanism for Super-diffusivity in Mouse Fibroblast Motility, *PLoS Comput. Biol.*, 2019, **15**(2), e1006732, DOI: 10.1371/journal.pcbi.1006732.

21 H. Shi, X. Wu, S. Sun, C. Wang, Z. Vangelatos, A. Ash-Shakoor, C. P. Grigoropoulos, P. T. Mather, J. H. Henderson and Z. Ma, Profiling the Responsiveness of Focal Adhesions of Human Cardiomyocytes to Extracellular Dynamic Nano-Topography, *Bioact. Mater.*, 2022, **10**, 367–377, DOI: 10.1016/j.bioactmat.2021.08.028.

22 A. Chen, D. K. Lieu, L. Freschauf, V. Lew, H. Sharma, J. Wang, D. Nguyen, I. Karakikes, R. J. Hajjar, A. Gopinathan, E. Botvinick, C. C. Fowlkes, R. A. Li and M. Khine, Shrink-film configurable multiscale wrinkles for functional alignment of human embryonic stem cells and their cardiac derivatives, *Adv. Mater.*, 2011, **23**(48), 5785–5791, DOI: 10.1002/adma.201103463.

23 Z. Zhao, J. Gu, Y. Zhao, Y. Guan, X. X. Zhu and Y. Zhang, Hydrogel Thin Film with Swelling-Induced Wrinkling Patterns for High-Throughput Generation of Multicellular Spheroids, *Biomacromolecules*, 2014, **15**(9), 3306–3312, DOI: 10.1021/bm500722g.

24 B. Priyadarshini, M. Rama, Chetan and U. Vijayalakshmi, Bioactive Coating as a Surface Modification Technique for Biocompatible Metallic Implants: A Review, *J. Asian Ceram. Soc.*, 2019, **7**(4), 397–406, DOI: 10.1080/21870764.2019.1669861.

25 A. M. Ziemba, T. D. Fink, M. C. Crochiere, D. L. Puhl, S. Sapkota, R. J. Gilbert and R. H. Zha, Coating Topologically Complex Electrospun Fibers with Nanothin Silk Fibroin Enhances Neurite Outgrowth *in Vitro*, *ACS Biomater. Sci. Eng.*, 2020, **6**(3), 1321–1332, DOI: 10.1021/acsbiomaterials.9b01487.

26 A. Dehghanghadikolaei and B. Fotovvati, Coating Techniques for Functional Enhancement of Metal Implants for Bone Replacement: A Review, *Materials*, 2019, **12**(11), 1795, DOI: 10.3390/ma12111795.

27 J. Song, B. Winkeljann and O. Lieleg, Biopolymer-Based Coatings: Promising Strategies to Improve the Biocompatibility and Functionality of Materials Used in Biomedical Engineering, *Adv. Mater. Interfaces*, 2020, **7**(17), 2000850, DOI: 10.1002/admi.202000850.

28 Q. Yang, J. Zhao, A. Muhammad, L. Tian, Y. Liu, L. Chen and P. Yang, Biopolymer Coating for Particle Surface Engineering and Their Biomedical Applications, *Mater. Today Bio*, 2022, **16**, 100407, DOI: 10.1016/j.mtbio.2022.100407.

29 H. zawa, Y. Toyoshima, M. Morimoto, H. Saimoto and S. Ifuku, Surface Wrinkles Induced on Oriented Chitosan Films *via* Horseradish Peroxidase-Catalyzed Reaction and Drying, *Chem. Lett.*, 2021, **50**(2), 252–255, DOI: 10.1246/CL.200740.

30 H. Izawa, N. Okuda, T. Yonemura, K. Kuroda, K. Ochi, S. Ifuku, M. Morimoto, H. Saimoto, M. Noda, K. Azuma, Y. Okamoto and N. Ito, Application of Bio-Based Wrinkled Surfaces as Cell Culture Scaffolds, *Colloids Interfaces*, 2018, **2**(2), 15, DOI: 10.3390/colloids2020015.

31 R. Wang, Y. Long, T. Zhu, J. Guo, C. Cai, N. Zhao and J. Xu, Fabrication of Oriented Wrinkles on Polydopamine/Polystyrene Bilayer Films, *J. Colloid Interface Sci.*, 2017, **498**, 123–127, DOI: 10.1016/j.jcis.2017.03.035.

32 Y. Wang, B. J. Kim, B. Peng, W. Li, Y. Wang, M. Li and F. G. Omenetto, Controlling Silk Fibroin Conformation for Dynamic, Responsive, Multifunctional, Micropatterned Surfaces, *Proc. Natl. Acad. Sci. U. S. A.*, 2019, **116**(43), 21361–21368, DOI: 10.1073/pnas.1911563116.

33 P. Petrini, C. Parolari and M. C. Tanzi, Silk Fibroin-Polyurethane Scaffolds for, *Tissue Eng.*, 2001, **2**, 849–854.

34 I. dal Prà, P. Petrini, A. Charini, S. Bozzini, S. Farè and U. Armato, Silk Fibroin-Coated Three-Dimensional Polyurethane Scaffolds for Tissue Engineering: Interactions with Normal Human Fibroblasts, *Tissue Eng.*, 2003, **9**(6), 1113–1121, DOI: 10.1089/10763270360728026.

35 X. Cheng, J. Fei, A. Kondyurin, K. Fu, L. Ye, M. M. M. Bilek and S. Bao, Enhanced Biocompatibility of Polyurethane-Type Shape Memory Polymers Modified by Plasma Immersion Ion Implantation Treatment and Collagen Coating: An *in Vivo* Study, *Mater. Sci. Eng., C*, 2019, **99**, 863–874, DOI: 10.1016/j.msec.2019.02.032.

36 S. L. Buffington, J. Paul, E. Ali, M. M. Macios, M. M. Mather and J. H. Henderson, Enzymatically triggered shape memory polymers, *Acta Biomater.*, 2019, **84**, 88–97, DOI: 10.1016/j.actbio.2018.11.031.

37 I. T. Garces, S. Aslanzadeh, Y. Boluk and C. Ayranci, Effect of Moisture on Shape Memory Polyurethane Polymers for Extrusion-Based Additive Manufacturing, *Materials*, 2019, **12**(2), 244, DOI: 10.3390/ma12020244.

38 A. Huot, T. Lefèvre, J.-F. Rioux-Dubé, F. Paquet-Mercier, A.-P. Nault, M. Auger and M. Pézolet, Effect of Mechanical Deformation on the Structure of Regenerated Bombyx Mori

Silk Fibroin Films as Revealed Using Raman and Infrared Spectroscopy, *Appl. Spectrosc.*, 2015, **69**(6), 689–698, DOI: 10.1366/14-07776.

39 H. Yang, S. Yang, J. Kong, A. Dong and S. Yu, Obtaining Information about Protein Secondary Structures in Aqueous Solution Using Fourier Transform IR Spectroscopy, *Nat. Protoc.*, 2015, **10**(3), 382–396, DOI: 10.1038/nprot.2015.024.

40 A. S. Lammel, X. Hu, S.-H. Park, D. L. Kaplan and T. R. Scheibel, Controlling Silk Fibroin Particle Features for Drug Delivery, *Biomaterials*, 2010, **31**(16), 4583–4591, DOI: 10.1016/j.biomaterials.2010.02.024.

41 X. Hu, D. Kaplan and P. Cebe, Determining beta-sheet crystallinity in fibrous proteins by thermal analysis and infrared spectroscopy, *Macromolecules*, 2006, **39**(18), 6161–6170, DOI: 10.1021/ma0610109.

42 B. Yang, W. M. Huang, C. Li and L. Li, Effects of Moisture on the Thermomechanical Properties of a Polyurethane Shape Memory Polymer, *Polymer*, 2006, **47**(4), 1348–1356, DOI: 10.1016/j.polymer.2005.12.051.

43 D. Kochhar, M. K. DeBari and R. D. Abbott, The Materiobiology of Silk: Exploring the Biophysical Influence of Silk Biomaterials on Directing Cellular Behaviors, *Front. Bioeng. Biotechnol.*, 2021, 9, DOI: 10.3389/fbioe.2021.697981.

44 A. Leal-Egaña and T. Scheibel, Interactions of Cells with Silk Surfaces, *J. Mater. Chem.*, 2012, **22**(29), 14330–14336, DOI: 10.1039/c2jm31174g.

45 S. H. Chaki, H. J. Joshi, J. P. Tailor and M. P. Deshpande, Study of SnS_2 Thin Film Deposited by Spin Coating Technique, *Mater. Res. Express*, 2017, **4**(7), 076402, DOI: 10.1088/2053-1591/aa72b6.

46 Y.-Y. Chang, B.-C. Jiang, P.-Y. Chen and Y.-Y. Chiang, An Affordable and Tunable Continuous Wrinkle Micropattern for Cell Physical Guidance Study, *J. Taiwan Inst. Chem. Eng.*, 2021, **126**, 288–296, DOI: 10.1016/j.jtice.2021.07.001.

47 J. Y. Chung, J. P. Youngblood and C. M. Stafford, Anisotropic Wetting on Tunable Micro-Wrinkled Surfaces, *Soft Matter*, 2007, **3**(9), 1163, DOI: 10.1039/b705112c.

48 J. Raasch, M. Ivey, D. Aldrich, D. S. Nobes and C. Ayranci, Characterization of Polyurethane Shape Memory Polymer Processed by Material Extrusion Additive Manufacturing, *Addit. Manuf.*, 2015, **8**, 132–141, DOI: 10.1016/j.addma.2015.09.004.

49 D. Zonoobi, *Mechanical Properties of Extrusion-Based Additive Manufacturing of Shape Memory Polymers*, MS thesis, University of Alberta, 2019, DOI: 10.7939/r3-eq6a-qe05.

50 A. Panin and A. Shugurov, Multi-Level Deformation of Thin Films Caused by Stress–Strain Distribution at the Film-Substrate Interface, *Procedia Eng.*, 2009, **1**(1), 23–26, DOI: 10.1016/j.proeng.2009.06.007.

51 A. Ojstršek, L. Jug and O. Plohl, A Review of Electro Conductive Textiles Utilizing the Dip-Coating Technique: Their Functionality, Durability and Sustainability, *Polymers*, 2022, **14**(21), 4713, DOI: 10.3390/polym14214713.

52 B. D. Lawrence, S. Wharram, J. A. Kluge, G. G. Leisk, F. G. Omenetto, M. I. Rosenblatt and D. L. Kaplan, Effect of Hydration on Silk Film Material Properties: Effect of Hydration on Silk Film Material Properties, *Macromol. Biosci.*, 2010, **10**(4), 393–403, DOI: 10.1002/mabi.200900294.

53 C. Mo, P. Wu, X. Chen and Z. Shao, The Effect of Water on the Conformation Transition of Bombyx Mori Silk Fibroin, *Vib. Spectrosc.*, 2009, **51**(1), 105–109, DOI: 10.1016/j.vibspec.2008.11.004.

54 Y. Cheng, L.-D. Koh, D. Li, B. Ji, M.-Y. Han and Y.-W. Zhang, On the Strength of β-Sheet Crystallites of Bombyx Mori Silk Fibroin, *J. R. Soc. Interface*, 2014, **11**(96), 20140305, DOI: 10.1098/rsif.2014.0305.

55 E. N. Sevcik, J. M. Szymanski, Q. Jallerat and A. W. Feinberg, Patterning on Topography for Generation of Cell Culture Substrates with Independent Nanoscale Control of Chemical and Topographical Extracellular Matrix Cues, *Curr. Protoc. Cell Biol.*, 2017, **75**(1), 10.23.1–10.23.25, DOI: 10.1002/cpcb.25.

56 M. Bril, S. Fredrich and N. A. Kurniawan, Stimuli-Responsive Materials: A Smart Way to Study Dynamic Cell Responses, *Smart Mater. Med.*, 2022, **3**, 257–273, DOI: 10.1016/j.smaim.2022.01.010.

57 J. Luo, M. Walker, Y. Xiao, H. Donnelly, M. J. Dalby and M. Salmeron-Sanchez, The Influence of Nanotopography on Cell Behaviour through Interactions with the Extracellular Matrix – A Review, *Bioact. Mater.*, 2022, **15**, 145–159, DOI: 10.1016/j.bioactmat.2021.11.024.

58 A. Leal-Egaña, G. Lang, C. Mauerer, J. Wickinghoff, M. Weber, S. Geimer and T. Scheibel, Interactions of Fibroblasts with Different Morphologies Made of an Engineered Spider Silk Protein, *Adv. Eng. Mater.*, 2012, **14**(3), B67–B75, DOI: 10.1002/adem.201180072.

59 K. Zhang, X. Mo, C. Huang, C. He and H. Wang, Electrospun Scaffolds from Silk Fibroin and Their Cellular Compatibility, *J. Biomed. Mater. Res.*, 2009, **9999A**, DOI: 10.1002/jbm.a.32497.

60 V. A. Schulte, M. Díez, M. Möller and M. C. Lensen, Surface Topography Induces Fibroblast Adhesion on Intrinsically Nonadhesive Poly(Ethylene Glycol) Substrates, *Biomacromolecules*, 2009, **10**(10), 2795–2801, DOI: 10.1021/bm900631s.

61 F. Wang, S. Xiao, S. Luo, Y. Fu, B. H. Skallerud, H. Kristiansen, M. Cui, C. Zhong, S. Liu, Y. Zhuo, J. He and Z. Zhang, Surface Wrinkling with Memory for Programming Adhesion and Wettability, *ACS Appl. Nano Mater.*, 2023, **6**(6), 4097–4104, DOI: 10.1021/acsanm.2c05410.

62 L. Yang, Q. Gao, L. Ge, Q. Zhou, E. M. Warszawik, R. Bron, K. W. C. Lai and P. Van Rijn, Topography Induced Stiffness Alteration of Stem Cells Influences Osteogenic Differentiation, *Biomater. Sci.*, 2020, **8**(9), 2638–2652, DOI: 10.1039/D0BM00264J.

63 M. Li, D. Joung, B. Hughes, S. D. Waldman, J. A. Kozinski and D. K. Hwang, Wrinkling Non-Spherical Particles and Its Application in Cell Attachment Promotion, *Sci. Rep.*, 2016, **6**(1), 30463, DOI: 10.1038/srep30463.

64 N. Bowden, S. Brittain, A. G. Evans, J. W. Hutchinson and G. M. Whitesides, Spontaneous Formation of Ordered Structures in Thin Films of Metals Supported on an Elastomeric Polymer, *Nature*, 1998, **393**(6681), 146–149, DOI: 10.1038/30193.

65 D. C. Hurley, M. Kopycinska-Müller, E. D. Langlois, A. B. Kos and N. Barbosa, Mapping Substrate/Film Adhesion with Contact-Resonance-Frequency Atomic Force Microscopy, *Appl. Phys. Lett.*, 2006, **89**(2), 021911, DOI: **10.1063/1.2221404**.

66 A. L. Volynskii, D. A. Panchuk, S. V. Moiseeva, A. S. Kechek'yan, A. I. Dement'ev, L. M. Yarysheva and N. F. Bakeev, New Approach to Evaluation of the Stress-Strain Properties of Nanolayers of Solid Materials, *Russ. Chem. Bull.*, 2009, **58**(5), 865–882, DOI: **10.1007/s11172-009-0110-7**.

67 K. G. Soans and C. Norden, Shining a Light on Extracellular Matrix Dynamics *in Vivo*, *Semin. Cell Dev. Biol.*, 2021, **120**, 85–93, DOI: **10.1016/j.semcdb.2021.05.008**.

68 S. Neuss, I. Blomenkamp, R. Stainforth, D. Boltersdorf, M. Jansen, N. Butz, A. Perez-Bouza and R. Knüchel, The Use of a Shape-Memory Poly(ε-Caprolactone)Dimethacrylate Network as a Tissue Engineering Scaffold, *Biomaterials*, 2009, **30**(9), 1697–1705, DOI: **10.1016/j.biomaterials.2008.12.027**.

69 K. A. Davis, X. Luo, P. T. Mather and J. H. Henderson, Shape Memory Polymers for Active Cell Culture, *JoVE*, 2011, **53**, 2903, DOI: **10.3791/2903**.

70 L.-F. Tseng, P. T. Mather and J. H. Henderson, Shape-Memory-Actuated Change in Scaffold Fiber Alignment Directs Stem Cell Morphology, *Acta Biomater.*, 2013, **9**(11), 8790–8801, DOI: **10.1016/j.actbio.2013.06.043**.

71 M. Ebara, K. Uto, N. Idota, J. Hoffman and T. Aoyagi, The Taming of the Cell: Shape-Memory Nanopatterns Direct Cell Orientation, *Int. J. Nanomed.*, 2014, 117, DOI: **10.2147/IJN.S50677**.

72 J. D. Kiang, J. H. Wen, J. C. Del Álamo and A. J. Engler, Dynamic and Reversible Surface Topography Influences Cell Morphology, *J. Biomed. Mater. Res.*, 2013, **101A**(8), 2313–2321, DOI: **10.1002/jbm.a.34543**.

73 J. N. Agyapong, B. Van Durme, S. Van Vlierberghe and J. H. Henderson, Surface Functionalization of 4D Printed Substrates Using Polymeric and Metallic Wrinkles, *Polymers*, 2023, **15**(9), 2117, DOI: **10.3390/polym15092117**.

74 M. A. Tomeh, R. Hadianamrei and X. Zhao, Silk Fibroin as a Functional Biomaterial for Drug and Gene Delivery, *Pharmaceutics*, 2019, **11**(10), 494, DOI: **10.3390/pharmaceutics11100494**.

75 N. Zubir and K. Pushpanathan, Silk in Biomedical Engineering: A Review, *Int. J. Eng. Invent.*, 2016, **5**(8), 18–29.

76 D. L. Puhl, J. L. Funnell, T. D. Fink, A. Swaminathan, M. Oudega, R. H. Zha and R. J. Gilbert, Electrospun Fiber-Mediated Delivery of Neurotrophin-3 MRNA for Neural Tissue Engineering Applications, *Acta Biomater.*, 2023, **155**, 370–385, DOI: **10.1016/j.actbio.2022.11.025**.

77 J. B. Nielsen, E. Benfeldt and R. Holmgaard, Penetration through the Skin Barrier, *Curr. Probl. Dermatol.*, 2016, **49**, 103–111, DOI: **10.1159/000441549**.

